Pergamon

J. Mech. Phys. Solids, Vol. 44, No. 11, pp. 1891–1928, 1996

0022–5096/96 $15.00+0.00

PII: S0022-5096(96)00047-6

THE INFLUENCE OF SCALE SIZE ON THE STABILITY OF PERIODIC SOLIDS AND THE ROLE OF ASSOCIATED HIGHER ORDER GRADIENT CONTINUUM MODELS

N. TRIANTAFYLLIDIS and S. BARDENHAGEN†

Aerospace Engineering Department, The University of Michigan, Ann Arbor, MI 48109, U.S.A.

(*Received* 25 *July* 1995; *in revised form* 26 *February* 1996)

ABSTRACT

Of interest here is the scale size effect on the stability of finitely strained, rate-independent solids with periodic microstructures. Using a multiple scales asymptotic technique, we express the critical load at the onset of the first instability and the corresponding eigenmode in terms of the scale size parameter ε. The zeroth order ε terms in these expansions depend on the standard (first order gradient) macroscopic moduli tensor, while all the higher order ε terms require the determination of higher order gradient macroscopic moduli. These macroscopic moduli, which are calculated by solving appropriate boundary value problems on the unit cell, relate the macroscopic (unit cell average) stress rate increment to the macroscopic displacement rate gradients.

The proposed general theory is subsequently applied to the investigation of the failure surfaces in periodic solids of infinite extent. For these solids one can define in macroscopic strain space a microscopic (local) failure surface, which corresponds to the onset of the first bulking-type instability in the solid, and a macroscopic (global) failure surface, which corresponds to the onset of the first long wavelength instability in the solid. The determination of the macrofailure surface is considerably easier than the determination of the microfailure surface, for it requires the calculation of the standard macroscopic moduli tensor. In addition, the regions where the two surfaces coincide is of significant practical interest, for a macroscopic localized mode of deformation (e.g. in the form of a shear band or a kink band) appears in the post-bifurcation regime. The prediction of these coincidence zones is based on a necessary criterion that depends on the higher order gradient macroscopic moduli.

A detailed example is given for the case of layered composites, in view of the possibility of obtaining closed form expressions for all the required macroscopic moduli and in view of the existence of an analytical solution to the microscopic failure problem. Two applications are presented, one for a foam rubber composite and another for a graphite–epoxy composite whose properties have been determined experimentally. Following the verification of the above mentioned necessary criterion for the coincidence of the micro- and macrofailure surfaces in the two examples, the presentation is concluded by a discussion and suggestions for further work. Copyright © 1996 Elsevier Science Ltd

1. INTRODUCTION AND MOTIVATION

The implication of the existence of two relevant scales—the microscopic (or representative cell) scale and the macroscopic (or overall structural dimension) scale—on the stability of mechanically-loaded media with internal structure, is an issue that appears repeatedly in engineering applications. For the case of quasistatic loading processes of interest here, the influence of the characteristic microstructural scale is

† Present address: Group T-3, MS B216, Los Alamos National Laboratory, Los Alamos, NM 87545, U.S.A.

reflected in the dependence of failure loads and modes on the size of the specimen, and the corresponding effect is termed "*scale effect*". Examples can be given over the entire spectrum of possible scales: atomic distance in crystals, dislocation spacing in metals, crystal size in polycrystalline aggregates, reinforcement size and spacing in composites and unit cell size in large space structures. As such we mention the stress-induced twinning and the shear localization in the deformation of crystals, the localization of deformation in compressed honeycombs and the kink band failure in fiber-reinforced composites under compression along the fiber direction. Over the last few decades, significant progress has been made in the derivation of averaged (macroscopic) theories from the underlying microstructures over a wide range of scales and material responses. These macroscopic theories ignore the microstructural scale size and their failure predictions cannot account for scale effects.

To correct this deficiency, a number of remedies have been proposed that involve the relaxation of the "*local action*" hypothesis of classical continuum mechanics, which dictates that only the first gradient of the deformation enters the constitutive law. Continuum models that violate the local action hypothesis are termed "*nonlocal*" and are divided into two classes: the first class consists of integral-type models whose strains and stresses at a given point depend on a convolution-type integral that accounts for the history of displacements or internal variables in a finite neighborhood about the point in question. The second class consists of pointwise models in which the stress calculation at a point is based exclusively on information given at this point. The simplest models in this class are higher order gradient models for which the strains and stresses at a point depend on the history of displacement or internal variable gradients, up to a certain order, evaluated at the point in question. Such models have been proposed for the localization of deformation in solids [see, e.g. Aifantis (1984), Triantafyllidis and Aifantis (1986)], but their origin can be traced back to the fluid mechanics literature (Van der Waals, 1893).

The above mentioned higher order gradient (usually second order) type models, although often physically motivated, are basically phenomenological. The coefficients of the second order displacement or internal variable gradient terms are either postulated [as for example in Triantafyllidis and Aifantis (1986) or in Muhlhaus and Aifantis (1991), respectively] or heuristically obtained from the assumption of continuum state equations coupling macroscopic and microscopic state variables [see, e.g. Mindlin (1964) and Aifantis (1987)]. With the recent considerable growth of higher order gradient models proposed for an ever increasing number of material behaviors, e.g. elastoplastic, viscoplastic, thermoviscoplastic, the issues of consistent derivation of the macroscopic model from the microscale one, and the role of the higher order gradient terms on the stability of the solid become increasingly relevant.

As a first step in this direction, Triantafyllidis and Bardenhagen (1993) have studied a discrete one-dimensional nonlinear elastic periodic microscopic model and consistently derived the corresponding continuum higher order displacement gradient models. The resulting simplest possible such model that takes the microstructural scale size into account (i.e. the lattice size) is the second order gradient one. This continuum model, derived from a given microstructure, has been found to give results in excellent agreement with corresponding discrete microscopic model for localized deformation solutions until the localization zone begins to propagate through the

structure. This work was subsequently generalized to two- and three-dimensional lattice structures by Bardenhagen and Triantafyllidis (1994), who derived the macroscopic higher order gradient terms in the continuum energy density of the lattice and examined their role on the stability of the infinite medium under finite strains.

The present work is motivated by the need to extend the above consistent derivations of non-local continuum macromodels, which include information on the scale size, to finitely strained, rate-independent periodic solids with continuum unit cells. Unlike the previously studied discrete lattice-type micromodels, the derivation of a non-local-type macroscopic continuum model is no longer possible due to the presence of internal variables and the possibility of local modes of deformation. However, it turns out that one can derive a consistent non-local model for the incremental response of the solid, which relates the macroscopic stress rate to the macroscopic displacement rate gradients of order n. The macroscopic moduli tensor for $n = 1$ is the standard homogenized moduli tensor of a periodic solid and is calculated by solving appropriate boundary value problems on the unit cell. The $n > 1$ higher order gradient macroscopic moduli tensors are also calculated by solving appropriate boundary value problems on the unit cell and are required for the determination of the scale dependence of the critical load and mode of mechanically-loaded periodic continua.

The outline of this paper is as follows. Section 2 presents the general theory for the scale size (denoted here by ε) dependence of the minimum eigenvalue and corresponding mode at the onset of the first buckling instability (the detailed derivations are given in Appendix A). A multiple scale asymptotic technique, proposed initially by Sanchez-Palencia (1974) for homogenization problems in linear elasticity, is appropriately modified for the linearized stability problem of interest. The zeroth order ε terms in these expansions depend on the standard (first order gradient) macroscopic moduli tensor, while all the higher order ε terms require the determination of higher order gradient macroscopic moduli. The symmetry properties for these macroscopic moduli tensors (up to the third order) are also discussed and the results are applied to the determination of the critical load in terms of ε.

In Section 3, the proposed general theory is applied to the investigation of the failure surfaces in periodic solids of infinite extent. For these solids one can define in macroscopic strain space a microscopic (local) failure surface, which corresponds to the onset of the first bifurcation instability in the solid, and a macroscopic (global) failure surface, which corresponds to the onset of the first long wavelength instability in the solid. The determination of the macrofailure surface, which requires the calculation of the loss of ellipticity for the standard macroscopic moduli tensor, is much easier than the determination of the microfailure surface, which requires Bloch wave-type calculations in the unit cell for all possible wave numbers [see Geymonant *et al.* (1993)]. In addition, the regions where the two surfaces coincide is of significant practical interest, for a macroscopic localization mode of deformation (e.g. in the form of a shear band or a kink band) appears in the post-bifurcation regime. The prediction of these coincidence zones is based on a necessary criterion which depends on the higher order gradient macroscopic moduli.

A detailed example is given for the case of layered composites in Section 4. The example choice is due to the possibility of closed form expressions for all the required macroscopic moduli and the existence of an analytical solution for the microscopic

failure problem (a brief outline of which is presented in Appendix B). Two applications are presented, one for a foam rubber composite under a state of finite biaxial strain and the other for a graphite–epoxy composite, whose properties have been determined experimentally, which is subjected to uniaxial compression. It is verified that the above mentioned criterion based on the higher order gradient macroscopic moduli, is indeed necessary for the coincidence between the micro- and macrofailure surfaces. Moreover, for the case of the rubber composite, the coincidence criterion in question is also a sufficient one, thus permitting the detection of all the macroscopic strain states in the composite that correspond to the onset of a kink band failure.

The presentation is concluded in Section 5 with a discussion of the above presented results and suggestions for further work.

2. GENERAL THEORY FOR SOLIDS WITH 3-D PERIODIC MICROSTRUCTURES

The goal of this work is to quantify the influence of scale size on the onset of failure in an arbitrarily-shaped, rate-independent solid with a perfectly periodic 3-D microstructure under quasistatic loading. For this class of solids, the onset of failure is identified with the appearance of the first buckling instability encountered during the loading process. Attention is focused on "*global*" modes of instability, i.e. modes that have a characteristic length several times larger than the size of the unit cell. This is an essential feature of the present investigation, for it enables us to use asymptotic development techniques to quantify the scale size dependence of the critical load and mode. To avoid the complication of mode interactions and multiple bifurcated equilibrium paths, it is further assumed that for the critical load of interest, the corresponding eigenmode is unique.

The approach that has been adopted in earlier work on scale size effects on the stability of discrete elastic media with regular microstructures [see Triantafyllidis and Bardenhagen (1993) and Bardenhagen and Triantafyllidis (1994)] and which is depicted in Fig. 1(a), is as follows. In Step 1 a macroscopic continuum energy density of the periodic medium is derived via an averaging technique in which the size ε of the microscale appears explicitly (in the terms involving the higher order gradients of the macroscopic deformation). In Step 2, a linearized stability analysis about the loading path of interest gives the wanted dependence of the minimum eigenvalue and corresponding eigenmode on the size of the microscale. Unfortunately this approach is no longer possible for the class of solids presently of interest and hence a different one has to be devised.

For rate-independent elastoplastic solids with a continuous microstructure, the difficulties lie in the first step (limiting process for scale size $\varepsilon \to 0$) of the above mentioned approach and are due to the following two reasons: the associated governing equations are nonlinear (due to constitutive and geometric effects) and the constitutive law is path dependent. Even in the absence of irreversible phenomena (elastic materials), the difficulties associated with the macroscopic response of a nonlinear periodic medium are due to the presence of local buckling modes, i.e. modes whose characteristic wavelength is of the order of the unit cell. Although a

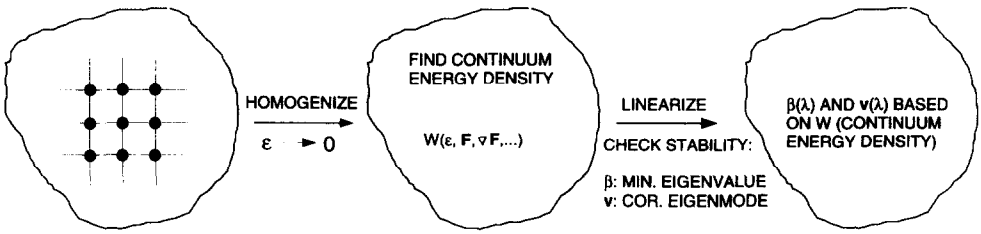

(a) DISCRETE MICROSTRUCTURES

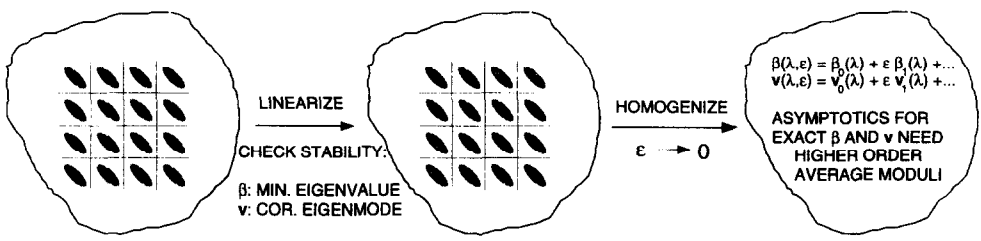

(b) CONTINUUM MICROSTRUCTURES

Fig. 1. The two approaches for taking into account scale size effects in the stability of media with periodic microstructures. The method used in (a) for discrete microstructures proceeds first with the homogenization of the solid and then with the linearization of the resulting non-local continuum. This approach is the one followed in all the stability analyses of microstructured media based on phenomenological non-local continuum models. The method proposed here for continuum microstructures in (b) reverses the order of homogenization and linearization and results with an asymptotic expansion for the minimum eigenvalue and eigenmode of the solid, the determination of which requires the calculation of the higher order gradient macroscopic moduli.

macroscopic energy density does exist [see Müller (1987)], obtaining an analytical expression for it is impossible for all practical purposes. Moreover, for inelastic materials the presence of internal variables—which are necessary for the modeling of irreversible processes—complicates an already hard homogenization task even further, due to difficulties associated with finding a finite number of macroscopic internal variables that can adequately describe the state of the unit cell.

The methodology most frequently used to find the macroscopic response of an inelastic microstructured solid, relies on an intuitive selection of the macroscopic internal variables based on certain assumptions about the response of the unit cell. This approximate technique, which has been successful in the derivation of simple macroscopic average theories which do not include scale size information [e.g. Gurson's (1977) model for porous elastoplastic solids], has recently been invoked in constructing phenomenological continuum plasticity theories that include scale size effects by Fleck and Hutchinson (1993). Consequently, the study of scale size effects on the stability of these solids has been based on such scale-dependent phenomenological models as in Leroy and Molinari (1993) for the case of elastic models, or as in Benallal and Tvergaard (1995) for the case of elastoplastic models.

Given that in the present work we are interested in the consistent derivation of

scale size effects on the onset of failure, we have to find an unambiguous methodology to eliminate the difficulties associated with the homogenization process. The proposed new methodology consists of simply reversing the order of Steps 1 and 2, as depicted in Fig. 1(b). Thus in Step 1 the exact linearized stability problem for the rate-independent elastoplastic continuum is established, which is obviously a function of the scale size ε. Subsequently in Step 2, a multiple scale asymptotic limiting process is used to find the wanted dependence of the minimum eigenvalue and corresponding eigenmode on the scale size ε. The advantage of interchanging the order of the steps used for discrete media is that there is a unique, consistent and unambiguous way to proceed for the continuous media considered here.

Some general comments are in order at this point. The derivation of the macroscopic continuum model from the underlying periodic continuum is the same in two or three dimensions. The general theory derivations in this section are presented in three dimensions, but the results for the two-dimensional case are easily recovered from their three-dimensional counterparts when the italic roman indexes $i, j, k, \ldots$ range from 1 to 2 (instead of 1 to 3). The Einstein summation convention over repeated italic roman indices is adopted in the rest of this work. Boldface symbols indicate tensor quantities while their components are denoted by the same symbol followed by the appropriate roman subscripts.

2.1. *Setting of the general stability problem*

Consider a solid which in its reference (undeformed) configuration occupies a volume V with boundary ∂V as seen in Fig. 2(a). The solid has a regular, perfectly periodic microstructure whose fundamental building block, termed the "unit cell", is shown in Fig. 2(b). If l is the size of the unit cell and if L is a characteristic overall dimension of the solid under study, the scale size ε is defined as $\varepsilon \equiv l/L$. Material points in the solid are identified by their position vector $\mathbf{X}$, while the current position vector of the same point is denoted by $\mathbf{x}$. The displacement of each material point $\mathbf{X}$ is denoted by $\mathbf{u}$ where $\mathbf{u} \equiv \mathbf{x}(\mathbf{X}) - \mathbf{X}$. The deformation gradient at $\mathbf{X}$, a quantity that measures the deformation in the neighborhood of each point, is denoted by $\mathbf{F} \equiv \mathrm{d}\mathbf{x}/\mathrm{d}\mathbf{X}$. The notation "$\mathrm{d}/\mathrm{d}\mathbf{X}$" is used rather than "$\partial/\partial\mathbf{X}$" to assist in distinguishing between derivation with respect to initial position $\mathbf{X}$, and derivation with respect to the macroscale variable, also denoted by $\mathbf{X}$, which is introduced in the multiple scales asymptotic analysis in Section 2.2.

The constitutive law obeyed by all rate-independent solids can be put in the following form

$$\dot{\Pi}_{ji}(\lambda, \mathbf{X}) = L_{ijkl}(\lambda, \mathbf{X})\dot{F}_{kl}, \tag{2.1}$$

where $\dot{\mathbf{\Pi}}$ is the rate of the first Piola–Kirchhoff stress, $\dot{\mathbf{F}} = \mathrm{d}\dot{\mathbf{u}}/\mathrm{d}\mathbf{X}$, is the rate of deformation gradient, its corresponding work conjugate quantity, and $\mathbf{L}$ is the incremental (or tangent) moduli tensor that characterizes the material's instantaneous response. Here by rate of a field quantity we denote its derivative with respect to any parameter that increases monotonically with the evolution of the loading process. The incremental moduli, i.e. the components of $\mathbf{L}$, depend obviously on position $\mathbf{X}$ as well as on the current state of the material point, which can be described by a set

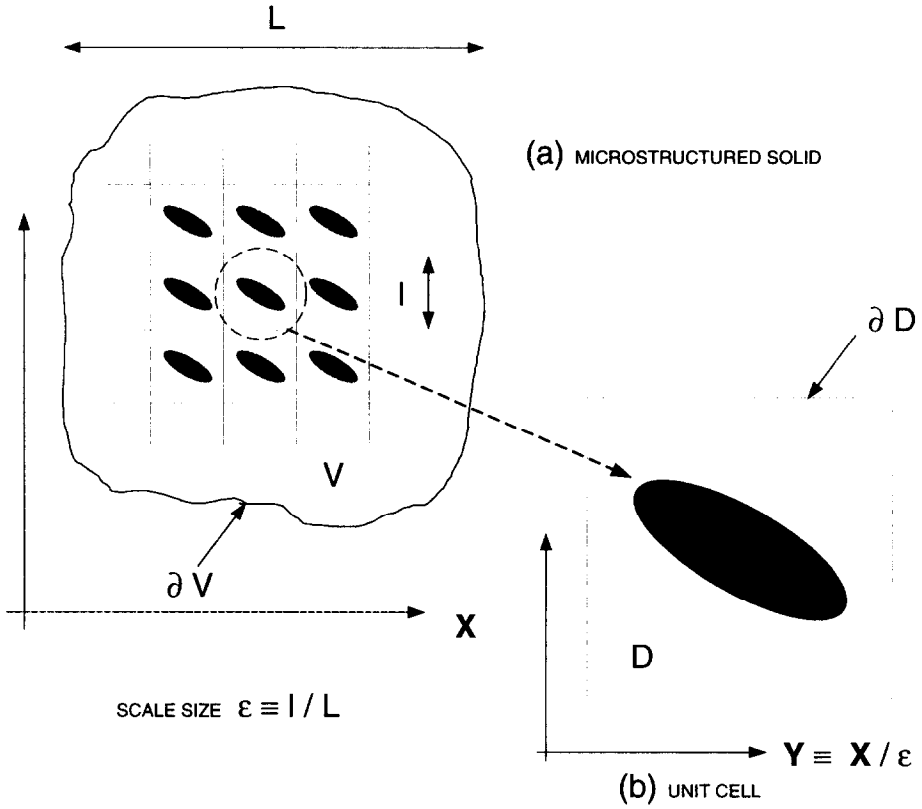

Fig. 2. The schematic representation of a solid with a periodic microstructure and the definition of the scale size parameter ε are shown in (a). The unit cell with its local coordinate system is shown enlarged in (b).

of internal variables. Every given loading process, assuming that it produces a unique response termed the "*principal equilibrium path*", can always be parameterized in terms of a scalar quantity λ, termed the "*load parameter*". Consequently and since all stresses and internal variables at a loading state characterized by λ can be expressed in terms of λ, the incremental moduli are also functions of λ as stated in (2.1). For the applications of interest here, the moduli tensor possesses the major symmetry, namely

$$L_{ijkl}(\lambda, \mathbf{X}) = L_{klij}(\lambda, \mathbf{X}). \tag{2.2}$$

Of interest here is the stability of the principal equilibrium path. For rate-independent elastoplastic solids, the issues of bifurcation and stability were first placed on a firm mathematical foundation by Hill (1958), who was able to give sufficient conditions for the exclusion of bifurcation in the incremental (rate one) problem of an elastoplastic solid and conjectured that these conditions should also guarantee uniqueness. He also investigated the condition for stability in elastoplastic problems by means of calculating the dissipation produced by small perturbations about the state in question and went on to show that his exclusion of rate one bifurcation criterion

was also sufficient for stability in the above described sense. Hill's stability criterion [which also implies exclusion of bifurcation in any rate along the principal branch—see Nguyen and Triantafyllidis (1989)] relies on the positive definiteness of a functional which is quadratic in the perturbation of the displacement rate $\delta\mathbf{v}(\mathbf{X})$.

Thus, the stability (or instability) of a loaded configuration, identified by λ, is characterized by the positive (or negative) sign of the minimum eigenvalue $\beta(\lambda)$ of the above mentioned Hill's stability functional which is defined by

$$\beta(\lambda) = \min_{\delta\mathbf{v}} \int_V L_{ijkl}(\lambda, \mathbf{X}) \frac{\mathrm{d}\delta v_i}{\mathrm{d}X_j} \frac{\mathrm{d}\delta v_k}{\mathrm{d}X_l} \mathrm{d}V, \quad \|\delta\mathbf{v}\|^2 = \delta v_i \delta v_i = 1, \tag{2.3}$$

where the minimum is taken over all kinematically admissible functions $\delta\mathbf{v}(\mathbf{X})$, i.e. all functions that are continuous and vanish at those points on the boundary ∂V where the displacement (essential) boundary conditions are prescribed. To avoid the scalar indeterminacy, it is further assumed that all admissible functions have unit norm. The assumed symmetry of the incremental moduli in (2.2) implies that $\beta(\lambda)$ is always a real number. To be consistent with our assumption on the beginning of Section 2 about the uniqueness of the critical mode, it will additionally be assumed that the wanted minimum $\beta(\lambda)$ is achieved for only one such admissible function which is denoted by $\mathbf{v}$ and, in view of (2.3), satisfies the following variational statement, equivalent to (2.3)

$$\int_V L_{ijkl}(\lambda, \mathbf{X}) \frac{\mathrm{d}v_k}{\mathrm{d}X_l} \frac{\mathrm{d}\delta v_i}{\mathrm{d}X_j} \mathrm{d}V = \beta(\lambda) \int_v v_i \delta v_i \mathrm{d}V, \tag{2.4}_1$$

whose pointwise form (Euler–Lagrange) is

$$\frac{\mathrm{d}}{\mathrm{d}X_j}\left[L_{ijkl} \frac{\mathrm{d}v_k}{\mathrm{d}X_l}\right] + \beta v_i = 0. \tag{2.4}_2$$

In any physically meaningful loading history, the solid under study is stable when no loads are applied to it, i.e. if $\lambda = \lambda_{\mathrm{in}}$ corresponds to the unloaded state of the solid, then $\beta(\lambda_{\mathrm{in}}) > 0$. As the loading is progressively applied, i.e. as the load parameter increases or decreases monotonically away from λ_{in}, $\beta(\lambda)$ decreases. The first instability of the solid that occurs during the prescribed loading path occurs at load λ_{c} and is detected from

$$\beta(\lambda_c) = 0, \quad \beta(\lambda) > 0 \quad \text{for} \quad |\lambda - \lambda_{\mathrm{in}}| < |\lambda_c - \lambda_{\mathrm{in}}|. \tag{2.5}$$

According to our previous assumption about the uniqueness of $\mathbf{v}(\lambda, \mathbf{X})$ corresponding to the $\beta(\lambda)$ [see comments pertaining to (2.4)], $\mathbf{v}(\lambda_{\mathrm{c}}, \mathbf{X})$ is the unique eigenmode corresponding to the first critical load λ_{c}. It should be also noted at this point that at the critical load of interest λ_{c}, the principal solution under investigation exhibits a buckling-type instability. Mathematically, this instability is either a bifurcation point or a limit load and the subsequent analysis does not require a distinction between the two cases. It is additionally assumed that $\beta(\lambda)$ is a smooth function of the load parameter, which from (2.5) implies

$$\frac{d\beta(\lambda_c)}{d\lambda}(\lambda_c - \lambda_{in}) < 0. \tag{2.6}$$

The above presented formulation for the linearized stability analysis of the finitely deformed, rate-independent, elastoplastic solid constitutes Step 1 in the proposed approach, according to Fig. 1(b). Obviously the minimum eigenvalue is a function of the scale size parameter ε, i.e. $\beta = \beta(\lambda, \varepsilon)$ and hence from (2.5) the critical load is a function of ε, i.e. $\lambda_c = \lambda_c(\varepsilon)$. It is exactly this dependence of the critical load on the scale size parameter that is sought, in an asymptotic form, in Step 2 of the proposed approach according to Fig. 1(b). Finding the scale size dependence of $\lambda_c(\varepsilon)$ requires the determination of the appropriate macroscopic (or average) moduli tensors. The order of these average moduli tensors depends on the number of terms required in the corresponding scale size expansion of the critical load, as will be seen in the following sections.

2.2. *Asymptotic analysis for minimum eigenvalue and eigenmode*

A multiple scale asymptotic technique, initially proposed by Sanchez-Palencia (1974), is the tool for obtaining the dependence of the critical load and mode on the scale size parameter. There are two different spatial coordinates that can be identified in this problem: the macroscopic scale parameter $\mathbf{X}$, which describes the global variation of the eigenmode and which pertains to the overall dimensions of the solid and a microscale coordinate parameter $\mathbf{Y}$ which describes the local variation of the eigenmode and which is defined by

$$\mathbf{Y} = \mathbf{X}/\varepsilon. \tag{2.7}$$

A key property of the microstructure is introduced at this point. A function defined on V is termed "*Y-periodic*" if it is periodic and assumes the same values on opposite faces of the parallelepiped unit cell. Since the microstructure of the solid is perfectly periodic, and considering principal loading paths that produce uniform macroscopic strain modes of deformation, we can additionally assume that the incremental moduli $\mathbf{L}(\lambda, \mathbf{X}) = L(\lambda, \mathbf{Y})$ are Y-periodic. In these new microscopic coordinates the unit cell is denoted by D and its boundary by ∂D [see Fig. 2(b)].

Next the asymptotic expansions for the minimum eigenvalue $\beta(\lambda, \varepsilon)$ and the corresponding eigenmode $\mathbf{v}(\lambda, \varepsilon, \mathbf{X})$ [see definition in (2.4)] are introduced. The asymptotic expansion for $\beta(\lambda)$ is taken to be

$$\beta(\lambda, \varepsilon) = \beta_0(\lambda) + \varepsilon\beta_1(\lambda) + \varepsilon^2\beta_2(\lambda) + \cdots. \tag{2.8}$$

The eigenmode's dependence on position $\mathbf{X}$ can be described on two scales, the macroscopic (global) dependence on $\mathbf{X}$ and the microscopic (local) dependence on $\mathbf{X}/\varepsilon = \mathbf{Y}$. In other words, we can put $\mathbf{v}(\lambda, \varepsilon, \mathbf{X}) = \mathbf{v}(\lambda, \varepsilon, \mathbf{X}, \mathbf{X}/\varepsilon) = \mathbf{v}(\lambda, \varepsilon, \mathbf{X}, \mathbf{Y})$, where $\mathbf{v}$ is Y-periodic and its asymptotic expansion with respect to ε is assumed to be

$$\mathbf{v}(\lambda, \varepsilon, \mathbf{X}) = \overset{0}{\mathbf{v}}(\lambda, \mathbf{X}, \mathbf{Y}) + \varepsilon\overset{1}{\mathbf{v}}(\lambda, \mathbf{X}, \mathbf{Y}) + \varepsilon^2\overset{2}{\mathbf{v}}(\lambda, \mathbf{X}, \mathbf{Y}) + \cdots. \tag{2.9}$$

The Y-periodicity of $\mathbf{v}$ implies the Y-periodicity of $\overset{i}{\mathbf{v}}$. In addition, a mode nor-

malization condition, which is a slight modification of the earlier mentioned $\|\mathbf{v}\| = 1$, is added [see comments on the general setting of the problem pertaining to (2.3)]

$$\int_v \overset{0}{v}_i \overset{0}{v}_i \mathrm{d}\mathbf{X} = \int_{\mathrm{X}} \left[\int_D v_i(\lambda, \varepsilon, \mathbf{X}, \mathbf{Y}) \overset{0}{v}_i(\lambda, \mathbf{X}, \mathbf{Y}) \mathrm{d}\mathbf{Y} \right] \mathrm{d}\mathbf{X} = 1. \tag{2.10}$$

All the ingredients are now in place to find the terms in the asymptotic expansions for the minimum eigenvalue and corresponding eigenmode. The starting point of these calculations is the variational equation that defines β and $\mathbf{v}$ in $(2.4)_1$. Substitution of (2.8), (2.9) in $(2.4)_1$, and subsequent expansion in powers of ε results in the following variational statements (See Appendix A for the complete derivations) which define β_i and $\overset{i}{\mathbf{v}}$ in terms of the various order macroscopic moduli—$\mathscr{L}(\lambda)$ (first order), $\mathscr{M}(\lambda)$ (second order), $\mathscr{N}(\lambda)$ (third order) and so on.

The variational statement for $\beta_0(\lambda)$ and the corresponding eigenmode $\overset{0}{\bar{\mathbf{v}}}(\lambda, \mathbf{X})$ and the definition for the first order macroscopic moduli tensor $\mathscr{L}(\lambda)$ are given by

$$\int_{\mathrm{X}} \left[\mathscr{L}_{ijpq}(\lambda) \frac{\partial \overset{0}{\bar{v}}_p}{\partial X_q} \frac{\partial \delta \bar{v}_i}{\partial X_j} - \beta_0(\lambda) \overset{0}{\bar{v}}_i \delta \bar{v}_i \right] \mathrm{d}\mathbf{X} = 0, \tag{2.11}_1$$

$$\mathscr{L}_{ijpq}(\lambda) \equiv \frac{1}{\mathrm{vol}\, D} \int_D \left[L_{ijkl}(\lambda, \mathbf{Y}) \left(\delta_{pk}\delta_{ql} + \frac{\partial \overset{pq}{\phi}_k}{\partial \mathbf{Y}_l} \right) \right] \mathrm{d}\mathbf{Y}. \tag{2.11}_2$$

Continuing with the next higher order terms, the variational statement for $\beta_1(\lambda)$ and $\overset{1}{\bar{\mathbf{v}}}(\lambda, \mathbf{X})$ and the definition of the second order macroscopic moduli tensor $\mathscr{M}(\lambda)$ are

$$\int_{\mathrm{X}} \left\{ \left[\mathscr{M}_{ijpqr}(\lambda) \frac{\partial^2 \overset{0}{\bar{v}}_p}{\partial X_q \partial X_r} \frac{\partial \delta \bar{v}_i}{\partial X_j} - \beta_1(\lambda) \overset{0}{\bar{v}}_i \delta \bar{v}_i \right] + \left[\mathscr{L}_{ijpq}(\lambda) \frac{\partial \overset{1}{\bar{v}}_p}{\partial X_q} \frac{\partial \delta \bar{v}_i}{\partial X_j} - \beta_0(\lambda) \overset{1}{\bar{v}}_i \delta \bar{v}_i \right] \right\} \mathrm{d}\mathbf{X} = 0, \tag{2.12}_1$$

$$\mathscr{M}_{ijpqr}(\lambda) \equiv \frac{1}{\mathrm{vol}\, D} \int_D \left[L_{ijkl}(\lambda, \mathbf{Y}) \left(\overset{pq}{\phi}_k(\lambda, \mathbf{Y}) \delta_{lr} + \frac{\partial \overset{pqr}{\psi}_k}{\partial Y_l} \right) \right] \mathrm{d}\mathbf{Y}. \tag{2.12}_2$$

The next terms of interest (and the last required for our applications as it will be seen subsequently) give the variational statement for $\beta_2(\lambda)$ and $\overset{2}{\bar{\mathbf{v}}}(\lambda, \mathbf{X})$ and the definition for the third order macroscopic moduli tensor $\mathscr{N}(\lambda)$

$$\int_{\mathrm{X}} \left\{ - \mathscr{N}_{ijspqr}(\lambda) \frac{\partial^3 \overset{0}{\bar{v}}_p}{\partial X_q \partial X_r \partial X_s} \frac{\partial \delta \bar{v}_i}{\partial X_j} - \beta_0(\lambda) \mathscr{S}_{ijpq}(\lambda) \frac{\partial \overset{0}{\bar{v}}_p}{\partial X_q} \frac{\partial \delta \bar{v}_i}{\partial X_j} - \beta_2(\lambda) \overset{0}{\bar{v}}_i \delta \bar{v}_i \right]$$

$$+ \left[\mathscr{M}_{ijpqr}(\lambda) \frac{\partial^2 \overset{1}{\bar{v}}^p}{\partial X_q \partial X_r \partial X_j} - \beta_1(\lambda) \overset{1}{\bar{v}}_i \delta \bar{v}_i \right] + \left[\mathscr{L}_{ijpq}(\lambda) \frac{\partial \overset{2}{\bar{v}}_p}{\partial X_q} \frac{\partial \delta \bar{v}_i}{\partial X_j} - \beta_0(\lambda) \overset{2}{\bar{v}}_i \delta \bar{v}_i \right] \right\} \mathrm{d}\mathbf{X} = 0, \tag{2.13}_1$$

$$\mathscr{N}_{ijspqr}(\lambda) \equiv -\frac{1}{\operatorname{vol} D}\int_D L_{ijkl}(\lambda, \mathbf{Y})\left(\overset{pqr}{\psi}_k \delta_{ls} + \frac{\partial \overset{pqrs}{\theta}_k}{\partial Y_l}\right)\Bigg]\mathrm{d}\mathbf{Y}, \tag{2.13}_2$$

$$\mathscr{S}_{ijpq}(\lambda) \equiv \frac{1}{\operatorname{vol} D}\int_D L_{ijkl}(\lambda, \mathbf{Y})\frac{\partial \overset{pq}{\zeta}_k}{\partial Y_l}\Bigg]\mathrm{d}\mathbf{Y}. \tag{2.13}_3$$

The Y-periodic functions $\overset{pq}{\boldsymbol{\phi}}(\mathbf{Y}), \overset{pqr}{\boldsymbol{\psi}}(\mathbf{Y}), \overset{pqrs}{\boldsymbol{\theta}}(\mathbf{Y})$ and $\overset{pq}{\boldsymbol{\zeta}}(\mathbf{Y})$ that appear in the expressions which define β_i and $\overset{i}{\mathbf{v}}$ as well as in the definitions of the various order macroscopic moduli are defined in Appendix A. The physical interpretation and some key symmetry properties of the above defined macroscopic moduli tensors of orders one to three is the object of the next section.

2.3. *Interpretation and properties of the macroscopic moduli*

In this section we give a physical interpretation of the macroscopic moduli tensors $\mathscr{L}(\lambda), \mathscr{M}(\lambda), \mathscr{N}(\lambda)$, introduced in $(2.11)_2$, $(2.12)_2$, $(2.13)_2$, respectively. We also provide equivalent expressions for these tensors, which are useful in the study of their symmetries.

From the microscopic constitutive equation for the solid $\dot{\Pi}_{ji} = L_{ijk}\dot{F}_{kl}$ where $\dot{F}_{kl} = \mathrm{d}\dot{u}_k/\mathrm{d}X_l$ [see (2.1)] and the microscopic incremental equilibrium $\mathrm{d}(L_{ijkl}(\mathrm{d}\dot{u}_k/\mathrm{d}X_l))/\mathrm{d}X_j = 0$ [which coincides with $(2.4)_2$ for $\beta = 0$] one can deduce the response of the solid to a deformation with a given average strain. By assuming a known macroscopic incremental displacement field $\overset{0}{\mathbf{v}}(\mathbf{X})$, i.e.

$$\frac{1}{\operatorname{vol} D}\int_D \dot{\mathbf{u}}(\mathbf{X}, Y)\mathrm{d}\mathbf{Y} = \overset{0}{\mathbf{v}}(\mathbf{X}) \tag{2.14}$$

and by invoking the same multiple scale asymptotic expansion for $\dot{\mathbf{u}}$ as in (2.9), one can easily repeat the analysis of the previous section for $\beta = 0$ to find that

$$\dot{\mathbf{u}} = \overset{0}{\mathbf{v}} + \varepsilon \overset{pq}{\boldsymbol{\phi}}(\mathbf{Y})\frac{\partial \overset{0}{\bar{v}}_p}{\partial X_q} + \varepsilon^2 \overset{pqr}{\boldsymbol{\psi}}(\mathbf{Y})\frac{\partial^2 \overset{0}{\bar{v}}_p}{\partial X_q \partial X_r} + \varepsilon^3 \overset{pqrs}{\boldsymbol{\theta}}(\mathbf{Y})\frac{\partial^3 \overset{0}{\bar{v}}_p}{\partial X_q \partial X_r \partial X_s} + \cdots. \tag{2.15}$$

Note that the absence of $\overset{i}{\mathbf{v}}(\mathbf{X})$ terms ($i \geqslant 1$) in (2.15) is due to the imposed constraint (2.14).

By introducing the expansion for $\dot{\mathbf{u}}$ (2.15) into the microscopic constitutive equation (2.1), namely $\dot{\Pi}_{ji} = L_{ijkl}(\lambda, \mathbf{Y})[(\partial/\partial X_l + \varepsilon^{-1}\partial/\partial Y_l)\dot{u}_k(\mathbf{X}, \mathbf{Y})]$ (where use is made of the chain rule of differentiation to replace $\mathrm{d}/\mathrm{d}X_i$ by $\partial/\partial X_i + \varepsilon^{-1}\partial/\partial Y_i$, see Appendix A) and subsequently averaging over the unit cell, one finds after some straightforward calculations

$$\frac{1}{\operatorname{vol} D}\int_D \dot{\Pi}_{ji}\mathrm{d}\mathbf{Y} = \mathscr{L}_{ijpq}\frac{\partial \overset{0}{\bar{v}}_p}{\partial X_q} + \varepsilon \mathscr{M}_{ijpqr}\frac{\partial^2 \overset{0}{\bar{v}}_p}{\partial X_q \partial X_r} + \varepsilon^2 \mathscr{N}_{ijspqr}\frac{\partial^3 \overset{0}{\bar{v}}_p}{\partial X_q \partial X_r \partial X_s} + \cdots, \tag{2.16}$$

where $\mathscr{L}$, $\mathscr{M}$, $\mathscr{N}$ are given by $(2.11)_2$, $(2.12)_2$ and $(2.13)_2$, respectively. The moduli tensor $\mathscr{L}$, which is the macroscopic first order gradient tensor, is the macroscopic tangent moduli tensor that gives within $O(\varepsilon^0)$ the relation between the macroscopic first Piola–Kirchhoff stress rate and the macroscopic first order deformation gradient rate $\partial \overset{0}{\dot{\mathbf{v}}}/\partial \mathbf{X}$. The moduli tensor $\mathscr{M}$, which is the macroscopic second order gradient moduli tensor, represents the scale size correction of $O(\varepsilon^1)$ in the above macroscopic constitutive law and depends on the macroscopic second order deformation gradient rate $\partial^2 \overset{0}{\dot{\mathbf{v}}}/\partial \mathbf{X} \partial \mathbf{X}$. Similarly $\mathscr{N}$ is the macroscopic third order gradient moduli tensor and so on. It should also be noted at this point that the expressions in $(2.11)_2$ for macroscopic first order gradient moduli, also termed homogenized moduli in the literature, have already been presented in the literature [see Sanchez-Palencia (1974) for the linear elastic case, Abeyaratne and Triantafyllidis (1984) for nonlinear hyperelastic materials] and used widely in applications. In contrast, the derivations for the higher order gradient moduli are presented here for the first time, since only phenomenological higher order gradient theories for microstructured continua have been presented in the literature so far.

At this stage alternative expressions for $\mathscr{L}$, $\mathscr{M}$, $\mathscr{N}$ are provided which are helpful in establishing their symmetries for arbitrary periodic microstructures. From the definition of $\overset{pq}{\boldsymbol{\phi}}$ in $(A.11)_2$ one can easily show that for any Y-periodic function $\mathbf{f}(\mathbf{Y})$

$$\int_D \frac{\partial f_i}{\partial Y_j} L_{ijkl}\left(\delta_{pk}\delta_{ql} + \frac{\partial \overset{pq}{\phi}_k}{\partial Y_l}\right) d\mathbf{Y} = 0. \tag{2.17}$$

Taking $\mathbf{f} = \overset{st}{\boldsymbol{\phi}}$ in (2.17) and combining with $(2.11)_2$ we obtain the following expression for $\mathscr{L}(\lambda)$

$$\mathscr{L}_{stpq}(\lambda) = \frac{1}{\text{vol}\, D}\int_D \left(\delta_{si}\delta_{tj} + \frac{\partial \overset{st}{\phi}_i}{\partial Y_j}\right) L_{ijkl}(\lambda, \mathbf{Y}) \left(\delta_{pk}\delta_{ql} + \frac{\partial \overset{pq}{\phi}_k}{\partial Y_l}\right) d\mathbf{Y}. \tag{2.18}$$

From the above expression for $\mathscr{L}$ follows that the macroscopic first order gradient moduli share the same major symmetry as the microscopic moduli, i.e. $L_{ijkl}(\lambda, \mathbf{Y}) = L_{klij}(\lambda, \mathbf{Y})$ and

$$\mathscr{L}_{stpq} = \mathscr{L}_{pqst}. \tag{2.19}$$

By taking $\mathbf{f} = \overset{stu}{\boldsymbol{\psi}}$ in (2.17) and recalling also the definition for $\overset{pqr}{\boldsymbol{\psi}}$ in $(A.16)_2$ one can obtain from $(2.12)_2$ the following expressions for the macroscopic second order gradient tensor $\mathscr{M}(\lambda)$

$$\mathscr{M}_{stpqr}(\lambda) = \frac{1}{\text{vol}\, D}\int_D L_{ijkl}(\lambda, \mathbf{Y}) \left[\overset{pq}{\phi}_k \delta_{lr}\left(\delta_{si}\delta_{tj} + \frac{\partial \overset{st}{\phi}_i}{\partial Y_j}\right) - \overset{st}{\phi}_k \delta_{lr}\left(\delta_{pi}\delta_{qj} + \frac{\partial \overset{pq}{\phi}_i}{\partial Y_j}\right)\right] d\mathbf{Y}. \tag{2.20}$$

From the major symmetry of $\mathbf{L}$ and (2.20) the following symmetries for $\mathscr{M}$ are deduced

$$\mathscr{M}_{stpqr} = -\mathscr{M}_{pqstr}. \tag{2.21}$$

By taking $\mathbf{f} = \overset{pqrs}{\boldsymbol{\theta}}$ in (2.17) and recalling also the definitions for $\overset{pqrs}{\boldsymbol{\theta}}$ in $(A.21)_2$ and for $\overset{pqr}{\boldsymbol{\psi}}$ in $(A.16)_2$, we obtain from $(2.13)_2$ the following expressions for the macroscopic third order gradient tensor $\mathscr{N}(\lambda)$

$$\mathscr{N}_{tuspqr}\lambda) = \frac{1}{\text{vol}\, D}\int_D L_{ijkl}(\lambda, \mathbf{Y})\left(\overset{pq}{\phi}_k \overset{tu}{\phi}_i \delta_{lr}\delta_{js} - \frac{\partial \overset{tus}{\psi}_i}{\partial Y_j}\frac{\partial \overset{pqr}{\psi}_k}{\partial Y_l}\right)\mathrm{d}\mathbf{Y}. \tag{2.22}$$

From (2.22) and the major symmetry of $\mathbf{L}$, the following symmetries for $\mathscr{N}$ are found

$$\mathscr{N}_{tuspqr} = \mathscr{N}_{pqrtus}. \tag{2.23}$$

2.4. *Unit cell symmetry and implications for macroscopic moduli*

The symmetries discussed in (2.19), (2.21), (2.23) are due to the major symmetry of the microscopic moduli [see (2.2)] and are valid for any periodic microstructure. In practice, the unit cell for most solids of interest enjoys some additional symmetries which are reflected in the above discussed macroscopic moduli. The simplest possible symmetry for the microstructure is the point symmetry of the unit cell with respect to its center, which if it exists initially at $\lambda = 0$, is preserved for all subsequent states of deformation resulting from an imposed arbitrary macroscopic deformation $\mathbf{F}(\lambda)$

$$\mathbf{L}(\lambda, \mathbf{Y}) = \mathbf{L}(\lambda, -\mathbf{Y}). \tag{2.24}$$

Notice that any Y-periodic function $\mathbf{f}$ can be decomposed in a sum of symmetric $\overset{S}{\mathbf{f}}$ and antisymmetric $\overset{A}{\mathbf{f}}$ functions, namely

$$f(\mathbf{Y}) = \overset{S}{\mathbf{f}}(\mathbf{Y}) + \overset{A}{\mathbf{f}}(\mathbf{Y}); \quad \overset{S}{\mathbf{f}}(\mathbf{Y}) \equiv \tfrac{1}{2}[\mathbf{f}(\mathbf{Y}) + \mathbf{f}(-\mathbf{Y})], \quad \overset{A}{\mathbf{f}}(\mathbf{Y}) \equiv \tfrac{1}{2}[\mathbf{f}(\mathbf{Y}) - \mathbf{f}(-\mathbf{Y})]. \tag{2.25}$$

From the above remark, and making use of (A.1), (A.2) and (2.24) one can show that

$$\overset{pq}{\boldsymbol{\phi}}(\mathbf{Y}) = -\overset{pq}{\boldsymbol{\phi}}(-\mathbf{Y}), \quad \overset{pqr}{\boldsymbol{\psi}}(\mathbf{Y}) = \overset{pqr}{\boldsymbol{\psi}}(-\mathbf{Y}), \quad \overset{pqrs}{\boldsymbol{\theta}}(\mathbf{Y}) = -\overset{pqrs}{\boldsymbol{\theta}}(-\mathbf{Y}). \tag{2.26}$$

Using (2.24), (2.26) in (2.20) one can easily conclude that for the point symmetric-type unit cell, the macroscopic second order gradient moduli vanish, i.e. if $\mathbf{L}(\lambda, \mathbf{Y}) = \mathbf{L}(\lambda, -\mathbf{Y})$ then

$$\mathscr{M}_{stpqr}(\lambda) = 0. \tag{2.27}$$

2.5. *Asymptotic analysis for the lowest critical load*

Following the asymptotic determination of the minimum eigenvalue $\beta(\lambda)$ of the solid's stability functional in (2.4) given in Sections 2.2–2.4, the dependence of the first critical load λ_c on the scale size parameter ε may now be found. The assumptions adopted in Section 2.1 about $\beta(\lambda)$ and λ_c are that in the neighborhood of λ_c the unique critical mode $\mathbf{v}(\lambda, \varepsilon, \mathbf{X})$ is global in nature and hence approaches $\overset{0}{\mathbf{v}}(\lambda, \mathbf{X})$ as $\varepsilon \to 0$ where

$\overset{0}{\mathbf{v}}$ is the eigenmode of the homogenized stability problem in (2.11). In this case the asymptotic dependence on λ_c on ε can be determined from the identity

$$\beta(\lambda_c, \varepsilon) = 0, \tag{2.28}$$

in which the critical load λ_c has the following asymptotic expansion in terms of ε

$$\lambda_c(\varepsilon) = \lambda_0 + \varepsilon\lambda_1 + \varepsilon^2\lambda_2 + \cdots. \tag{2.29}$$

Combining (2.8), (2.28), (2.29) one easily deduces

$$\begin{aligned} &\beta_0(\lambda_0) = 0, \\ &\lambda_1 = -\beta_1(\lambda_0)/[\mathrm{d}\beta_0/\mathrm{d}\lambda]_0, \\ &\lambda_2 = -[\beta_2(\lambda_0) + [\mathrm{d}\beta_1/\mathrm{d}\lambda]_0\lambda_1 + 0.5[\mathrm{d}^2\beta_0/\mathrm{d}\lambda^2]_0\lambda_1^2]/[\mathrm{d}\beta_0/\mathrm{d}\lambda]_0, \end{aligned} \tag{2.30}$$

where the 0 subscript denotes evaluation of the bracketed quantity at $\lambda = \lambda_0$. In view of $(2.30)_1$ and the assumptions about the eigenmode corresponding to $\beta(\lambda)$ as $\varepsilon \to 0$, λ_0 is from (2.11) the first critical load of the homogenized solid.

At this point it is worthwhile recording the expressions for $[\mathrm{d}\beta_0/\mathrm{d}\lambda]_0$, $\beta_1(\lambda_0)$ and $\beta_2(\lambda_0)$ in terms of the homogenized higher order gradient moduli. A straightforward differentiation of $(2.11)_1$ with respect to λ combined with the choice $\delta\bar{v}_i = \overset{0}{\bar{v}}_i$ gives, in view of the $O(\varepsilon^0)$ term in the normalization condition (2.10) $\int_{\mathbf{X}} [\overset{0}{\bar{v}}_i \overset{0}{\bar{v}}_i] \mathrm{d}\mathbf{X} = 1$

$$[\mathrm{d}\beta_0/\mathrm{d}\lambda]_0 = \int_{\mathbf{X}} \left\{ [\mathrm{d}\mathscr{L}_{ijpq}/\mathrm{d}\lambda]_0 \frac{\partial \overset{0}{\bar{v}}_p}{\partial X_q} \frac{\partial \overset{0}{\bar{v}}_i}{\partial X_j} \right\} \mathrm{d}\mathbf{X}. \tag{2.31}$$

By taking $\delta\bar{v}_i = \overset{0}{\bar{v}}_i$ in (2.12), and $\delta\bar{v}_i = \overset{1}{\bar{v}}_i$ in $(2.11)_1$, one can easily deduce, in view also of the previously discussed normalization condition for $\overset{0}{\mathbf{v}}$, the following expression for $\beta_1(\lambda_0)$

$$\beta_1(\lambda_0) = \int_{\mathbf{X}} \left[\mathscr{M}_{ijpqr}(\lambda_0) \frac{\partial^2 \overset{0}{\bar{v}}_p}{\partial X_q X_r} \frac{\partial \overset{0}{\bar{v}}_i}{\partial X_j} \right] \mathrm{d}\mathbf{X}. \tag{2.32}$$

Similarly by taking $\delta\bar{v}_i = \overset{0}{\bar{v}}_i$ in $(2.13)_1$, $\delta\bar{v} = \overset{1}{\bar{v}}_i$ in $(2.12)_1$ and $\delta\bar{v}_i = \overset{2}{\bar{v}}_i$ in $(2.11)_1$, in conjunction with the previously discussed normalization condition for $\overset{0}{\mathbf{v}}$, and recalling from $(2.30)_1$ that $\beta_0(\lambda_0) = 0$, $\beta_2(\lambda_0)$ takes the form

$$\beta_2(\lambda_0) = \int_{\mathbf{X}} \left[-\mathscr{N}_{ijspqr}(\lambda_0) \frac{\partial^3 \overset{0}{\bar{v}}_p}{\partial X_q \partial X_r \partial X_s} \frac{\partial \overset{0}{\bar{v}}_i}{\partial X_j} - \mathscr{L}_{ijpq}(\lambda_0) \frac{\partial \overset{1}{\bar{v}}_p}{\partial X_q} \frac{\partial \overset{1}{\bar{v}}_i}{\partial X_j} \right] \mathrm{d}\mathbf{X}. \tag{2.33}$$

For the point-symmetric microstructures discussed in (2.24), one can easily see that since from (2.27) $\mathscr{M} = \mathbf{0}$, this implies from (2.32) that $\beta_1 = 0$ and from $(2.12)_1$ and the orthogonality condition $\int_{\mathbf{X}} [\overset{1}{\bar{v}}_i \overset{0}{\bar{v}}_i] \, \mathrm{d}\mathbf{X} = 0$ [$O(\varepsilon)$ term in (2.10)] that $\overset{1}{\mathbf{v}} = 0$. Consequently (2.32), (2.33) for the symmetric unit cells, i.e. for $\mathbf{L}(\lambda, \mathbf{Y}) = \mathbf{L}(\lambda, -\mathbf{Y})$ simplify to

$$\beta_1(\lambda_0 = 0, \quad \beta_2(\lambda_0) = \int_{\mathbf{X}} \left[-\mathscr{N}_{ijspqr}(\lambda_0) \frac{\partial^3 \overset{0}{\tilde{v}}_p}{\partial X_q \partial X_r \partial X_s} \frac{\partial \overset{0}{\tilde{v}}_i}{\partial X_j} \right] d\mathbf{X}. \tag{2.34}$$

The determination of $\beta_0(\lambda_0), \overset{0}{\tilde{v}}_i$, and subsequently that of $\beta_1(\lambda_0)$ or $\beta_2(\lambda_0)$, requires the specification of macroscopic boundary conditions for the macroscopic boundary value problems $(2.11)_1$, $(2.12)_1$, etc. In the absence of boundary layers, i.e. as long as the asymptotic expansions for the eigenmode in (2.9) are valid for all $\mathbf{X}$ in the boundary ∂V, the task of finding the appropriate macroscopic boundary conditions is straightforward. The required modifications for the general theory in the presence of boundary layers are rather involved and depend on the particular nature of each boundary problem considered and thus will not be addressed here.

3. APPLICATIONS TO PERIODIC SOLIDS OF INFINITE EXTENT

The above presented general theory, which uses higher order gradient macroscopic moduli to quantify the effect of scale size on the first critical load in periodic composites, has been developed for finite solids. For the special case where the boundary effects can be ignored (solids of infinite extent), the theory has a very interesting application in determining the regions where the macrofailure surface of the composite does not coincide with the microfailure surface (the definitions for these failure surfaces are given immediately below). The regions of coincidence between the micro- and macrofailure surfaces are of interest since they identify the macroscopic strain states at which an initially global mode of deformation develops into a macroscopically localized mode of failure (of the shear band or kink band type).

3.1. *Micro- versus macrofailure surface for a periodic composite*

The definition of failure in composites is an extremely difficult task, due to the complexity and multiplicity of physical mechanisms that contribute to their failure. For the case of ductile solids with periodic microstructures, which are loaded primarily in compression, their ultimate failure can be related to the onset of a buckling mode. Consequently, one can define as onset of failure the occurrence of the first bifurcation away from the periodic solution in which all cells deform identically. The determination of these theoretical failure surfaces for periodic media of infinite extent, when they are subjected to a macroscopic deformation gradient $\mathbf{F}$ can be done as follows.

The macroscopically applied deformation gradient $\mathbf{F}$ is parameterized in terms of a scalar parameter λ such that $\mathbf{F}(\lambda_{\text{in}}) = \mathbf{I}$ and the principal stretches $\lambda_i(\lambda)$ corresponding to $\mathbf{F}(\lambda)$ change monotonically from their initial values $\lambda_i(\lambda_{\text{in}}) = 1$, as λ moves monotonically away from λ_{in}. The stability parameter $\beta(\lambda)$ is the minimum eigenvalue of the quotient of the two quadratic forms defined in $(2.4)_1$. Following the work of Geymonant *et al.* (1993), it can be shown that the eigenmode $\mathbf{v}(\lambda, \mathbf{X})$ which corresponds to $\beta(\lambda)$, is always of the form $\mathbf{v}(\lambda, \mathbf{X}) = \mathbf{p}(\mathbf{Y}) \exp[i\boldsymbol{\omega} \cdot \mathbf{Y}]$† where $\mathbf{p}(\mathbf{Y})$ is a

† These solutions to linear equations with periodic coefficients in two or three dimensions, go in the physics literature by the name of "Bloch waves" (in one dimension they are termed "Floquet waves").

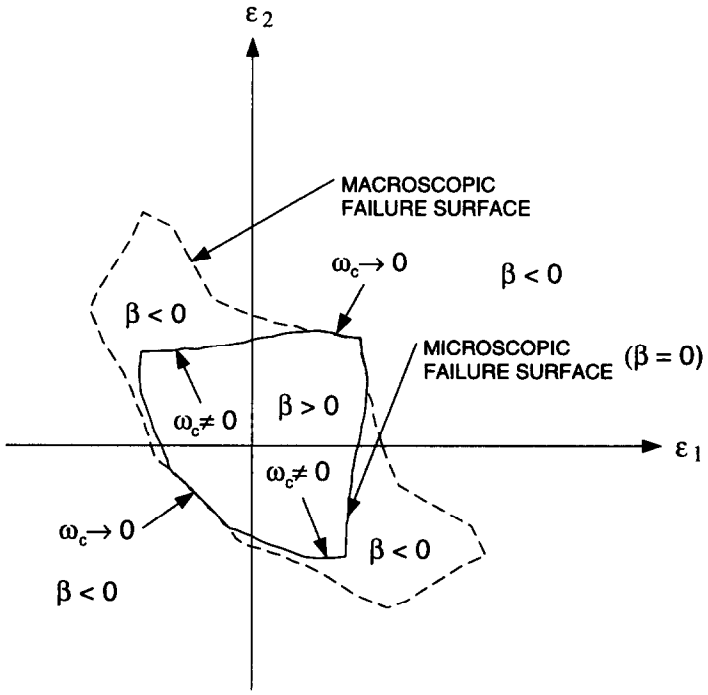

Fig. 3. Typical example of the micro- (onset of bifurcation) and macro- (loss of ellipticity of the homogenized moduli) failure surfaces for a periodic composite which is subjected to a state of macroscopic finite biaxial strain ε_1, ε_2, where $\varepsilon_i = \ln(\lambda_i)$. All strain states inside the microfailure surface correspond to stable periodic principal solutions. The points of coincidence of the two surfaces are characterized by infinitely long critical wavelengths $\omega_c \to 0$ and correspond to the onset of failure by a macroscopic localization mode.

Y-periodic function and $\boldsymbol{\omega}$ the corresponding wavenumber vector. Following the discussion of Section 2.1 [see also (2.5)], the first bifurcation occurs at λ_c for which $\beta(\lambda_c) = 0$ while the corresponding wavenumber vector is $\boldsymbol{\omega}_c$.

One can display the thus obtained stability results by plotting the onset of failure surface in the space spanned by the principal values of the applied macroscopic $\mathbf{F}$. Thus for a two-dimensional periodic composite and under the assumption of fixed principal axes, i.e. for $\mathbf{F} = \text{diag}[\lambda_1, \lambda_2]$, the onset of failure surface consisting of all pairs $\{\lambda_1(\lambda_c), \lambda_2(\lambda_c)\}$ will look something like the solid curve in Fig. 3 [which has been calculated for an infinite planar, nonlinear, periodic truss by Schraad and Triantafyllidis (1996)]. All points inside (outside) the solid line have $\beta(\lambda) > 0$ $\beta(\lambda) < 0$), thus indicating that the corresponding macroscopic deformations $\mathbf{F}(\lambda)$ are stable (unstable) against buckling.

The above obtained onset of failure surface is termed the microscopic (or local) failure surface, for it corresponds to the onset of first instability occurring in the infinite periodic medium loaded by $\mathbf{F}$. The components of $\boldsymbol{\omega}_c$ are the dimensionless wavenumbers of the corresponding bifurcation eigenmode, i.e. they are the ratios of the cell size to the wavelengths of the eigenmode along the coordinate directions. If the characteristic wavelength of the eigenmode at the onset of the first instability is commensurate with the unit cell size ε, i.e. $\boldsymbol{\omega}_c \neq 0$, then the onset of failure mode is local in nature.

It is conceivable that the onset of failure mode has characteristic wavelength much larger than the unit cell size ε, i.e. $\omega_c \to 0$, in which case the onset of failure mode is macroscopic (or global) in nature. If this is the case, it has been shown by Geymonant *et al.* (1993), that λ_c can be found from macroscopic considerations, i.e. by determining the loss of ellipticity of the homogenized (macroscopic) incremental moduli of the solid $\mathscr{L}(\lambda)$ defined in (2.18). Specifically, if $\omega_c \to 0$, then there exist unit vectors $\boldsymbol{\alpha}^c$, $\mathbf{n}^c$ such that $\mathscr{L}_{ijkl}(\lambda_c)\alpha_i^c n_j^c \alpha_k^c n_l^c = 0$ while for all other unit vectors $\boldsymbol{\alpha}$, $\mathbf{n}$ and any $|\lambda - \lambda_{in}| \leqslant |\lambda_c - \lambda_{in}|$, $\mathscr{L}_{ijkl}(\lambda)\alpha_i n_j \alpha_k n_l > 0$. For the same two-dimensional periodic composite, under an applied $\mathbf{F}$ with fixed principal directions, the above defined macroscopic failure surface will be something like the dotted curve in Fig. 3. From the above discussion it is evident that the microscopic failure surface lies always inside the macroscopic failure surface, with the two surfaces coinciding when the eigenmode corresponding to first bifurcation is global in nature, i.e. $\omega_c \to 0$.

The locus of points in $\mathbf{F}$ space where the two failure surfaces coincide is of particular interest in this work for two reasons. First, it determines the region of validity of the homogenization theory since for the macroscopic strains in question no local instability precedes the global one. Second, as it will be argued subsequently, if the first instability of the periodic medium is macroscopic in nature, the post-buckling failure mode is likely to develop into a macroscopically localized mode of failure (of the shear band or kink band type). The determination of the regions of $\mathbf{F}$ where the macro- and microfailure surfaces do not coincide is permitted by calculations involving the higher order gradient homogenized moduli, as it will be subsequently discussed.

3.2. *Micro- and macrofailure surface separation criterion*

Given the unit cell geometric and material properties of a rate-independent periodic solid, one can easily calculate for each macroscopic deformation state $\mathbf{F}(\lambda)$ the macroscopic homogenized moduli $\mathscr{L}(\lambda)$ according to (2.11). The determination of the macroscopic failure surface for the infinite periodic solid follows directly from the investigation of the loss of ellipticity of $\mathscr{L}(\lambda)$, as discussed in the previous subsection. The calculation of the corresponding microscopic failure surface based on the Bloch wave theory—also outlined in the previous subsection—is a much more computationally intensive task, for it requires the stability investigation of the medium for all possible wavenumber vectors $\boldsymbol{\omega}$ at each $\mathbf{F}(\lambda)$.

So far, the only way to determine where the two failure surfaces coincided was to calculate the more difficult—and computationally considerably more time consuming—microscopic failure surface and determine the points on that surface for which the corresponding critical wavenumber was approaching zero. We propose, and subsequently verify, a new criterion which is based on the calculation of $\beta_1(\lambda_0)$ $[\beta_2(\lambda_0)]$, which finds the scale size effect on the macrofailure mode and thus indicates the existence of a prior microfailure mode. Note that for the infinite problem the scale size parameter is the (finite) ratio of the unit cell size to the characteristic length of the eigenmode $\mathbf{v}$ which, although much larger than the unit cell size, is considered finite.

We propose (with justification, but without proof) the following necessary criterion for the separation of the micro- and macrofailure surfaces in a periodic composite,

based on the sign of $\beta_1(\lambda_0)$ [or $\beta_2(\lambda_0)$] for asymmetric (or symmetric) microstructures. If $\beta_1(\lambda_0) < 0$ [or $\beta_2(\lambda_0 < 0]$, the inclusion of the scale size effect reveals that the minimum eigenvalue is negative at the macrofailure load λ_0. In this case there must be a local eigenmode (whose size is of the order of the size of the unit cell), which precedes the occurrence of the macroscopic eigenmode. The criterion, being a sufficient one, does not always work the other way around, i.e. if $\beta_1(\lambda_0) > 0$ [or $\beta_2(\lambda_0) > 0$], it cannot be guaranteed that the first critical eigenmode is a global one. A verification of the proposed criterion which is based on the sign of $\beta_1(\lambda_0)$ [or $\beta_2(\lambda_0)$] will be given in Section 4 for two different laminated composites.

The determination of β_1 (β_2 if $\beta_1 = 0$) [or equivalently of $\lambda_1(\lambda_2$ if $\lambda_1 = 0)$] for the infinite periodic solid, follows from the general theory developed in Section 2.5. Consider a periodic composite under a macroscopic deformation $\mathbf{F}(\lambda)$ whose homogenized moduli $\mathscr{L}$ first lose ellipticity at λ_0 along direction $\mathbf{n}$, i.e.

$$[\mathscr{L}_{ijkl}(\lambda_0)n_k n_l]\overset{0}{\bar{\alpha}}_k = 0 \quad (\|\mathbf{n}\| = \|\overset{0}{\bar{\boldsymbol{\alpha}}}\| = 1). \tag{3.1}$$

The matrix $\mathscr{L}_{ijkl}(\lambda_0)n_k n_l$ is positive semi-definite with unit eigenvector $\overset{0}{\bar{\boldsymbol{\alpha}}}$. For any unit vector $\mathbf{m} \neq \mathbf{n}$, $\mathscr{L}_{ijkl}(\lambda_0)m_k m_l$ is positive definite. Also $\mathscr{L}_{ijkl}(\lambda)m_k m_l$ is positive definite for all $|\lambda - \lambda_{\text{in}}| < |\lambda_0 - \lambda_{\text{in}}|$ and all unit vectors $\mathbf{m}$. The (macroscopic) eigenmode corresponding to this failure mode is

$$\overset{0}{\bar{v}}_i = \overset{0}{\bar{\alpha}}_i f(z); \quad z \equiv n_k X_k. \tag{3.2}$$

From (3.1) and since $\beta_0(\lambda_0) = 0$ [see $(2.30)_1$] one can easily verify that the eigenmode (3.2) satisfies the Euler–Lagrange equations for the eigenmode $(2.11)_1$, namely $\partial/\partial X_j[\mathscr{L}_{ijkl}(\lambda_0)\partial\overset{0}{\bar{v}}_k/\partial X_l] = 0$.

The next order term in the expansion of the critical load requires, according to $(2.30)_2$, the calculation of $\beta_1(\lambda_0)$ which is given by (2.32). Using (3.2), as well as the symmetry properties of $\mathscr{M}(\lambda)$ [see (2.21)], it can be shown that $\lambda_1 = \beta_1(\lambda_0) = 0$. Indeed†

$$\beta_1(\lambda_0) = \mathscr{M}_{ijpqr}(\lambda_0)\overset{0}{\bar{\alpha}}_i\overset{0}{\bar{\alpha}}_p n_j n_q n_r \int_{\mathbf{X}} \frac{\mathrm{d}f}{\mathrm{d}z}\frac{\mathrm{d}^2 f}{\mathrm{d}z^2}\mathrm{d}\mathbf{X} \Big/ \int_{\mathbf{X}} f^2 \mathrm{d}\mathbf{X} = 0, \tag{3.3}$$

since

$$\mathscr{M}_{ijpqr}(\lambda_0)\overset{0}{\bar{\alpha}}_i\overset{0}{\bar{\alpha}}_p n_j n_q n_r = \mathscr{M}_{pqijr}(\lambda_0)\overset{0}{\bar{\alpha}}_p\overset{0}{\bar{\alpha}}_i n_q n_j n_r = -\mathscr{M}_{ijpqr}(\lambda_0)\overset{0}{\bar{\alpha}}_i\overset{0}{\bar{\alpha}}_p n_j n_q n_r = 0.$$

Since $\lambda_1 = 0$, the calculation of the scale size effect on the critical load requires λ_2 for which, according to $(2.30)_3$, $\beta_2(\lambda_0)$ must be determined. Notice from the expression (2.33) for $\beta_2(\lambda_0)$, that $\overset{1}{\bar{\mathbf{v}}}(\mathbf{X})$ is also required. This term is found from $(2.12)_1$, whose Euler–Lagrange equation—in view of the simplification $\beta_0(\lambda_0) = \beta_1(\lambda_0) = 0$—takes the form

† For the infinite solid $\mathbf{X}$ denotes the entire three-dimensional space. Moreover the normalization condition $\int_{\mathbf{X}}[\overset{0}{\bar{v}}_i\overset{0}{\bar{v}}_i]\mathrm{d}\mathbf{X} = 1$ is replaced by the amplitude normalization $\overset{0}{\bar{\alpha}}_i\overset{0}{\bar{\alpha}}_i = 1$ [see (2.8)]. It is tacitly assumed that $\int_{\mathbf{X}} f^2\mathrm{d}\mathbf{X}$, $\int_{\mathbf{X}}(\mathrm{d}f/\mathrm{d}z)^2\mathrm{d}\mathbf{X}$ over the entire space are finite.

$$\frac{\partial}{\partial X_j}\left[\mathscr{L}_{ijpq}(\lambda_0)\frac{\partial \overset{1}{\bar{v}}_p}{\partial_q}\right] = -\frac{\partial}{\partial X_j}\left[\mathscr{M}_{ijpqr}(\lambda_0)\frac{\partial^2 \overset{0}{\bar{v}}_p}{\partial X_q \partial X_r}\right]. \tag{3.4}$$

The solution to (3.4) is

$$\overset{1}{\bar{v}}_i = \overset{1}{\bar{\alpha}}_i \frac{\mathrm{d}f}{\mathrm{d}z}, \quad [\mathscr{L}_{ijpq}(\lambda_0)n_j n_q]\overset{1}{\bar{\alpha}}_p = -\mathscr{M}_{ijpqr}(\lambda_0)\overset{0}{\bar{\alpha}}_p n_j n_q n_r \equiv g_i. \tag{3.5}$$

The linear equation $(3.5)_2$ always admits a solution $\overset{1}{\bar{\boldsymbol{\alpha}}}$ since its right hand side $g_i \equiv -\mathscr{M}_{ijpqr}(\lambda_0)\overset{0}{\bar{\alpha}}_p n_j n_q n_r$ satisfies the compatibility condition $g_i \overset{0}{\bar{\alpha}}_i = 0$ [see $(3.3)_2$], and eigenvector $\overset{0}{\bar{\boldsymbol{\alpha}}}$ is unique. By using (3.2) and (3.5) in the expression (2.33) for $\beta_2(\lambda_0)$ we obtain

$$\beta_2(\lambda_0) = [\mathscr{N}_{ijspqr}(\lambda_0)\overset{0}{\bar{\alpha}}_i \overset{0}{\bar{\alpha}}_p n_j n_s n_q n_r - \mathscr{L}_{ijpq}(\lambda_0)\overset{1}{\bar{\alpha}}_i \overset{1}{\bar{\alpha}}_p n_j n_q]G;$$

$$G \equiv \int_{\mathrm{X}} -\frac{\mathrm{d}^3 f}{\mathrm{d}z^3}\frac{\mathrm{d}f}{\mathrm{d}z}\mathrm{d}\mathbf{X} \Big/ \int_{\mathrm{X}} f^2 \mathrm{d}\mathbf{X}. \tag{3.6}$$

The sign of $\beta_2(\lambda_0)$ is determined by the bracketed term since $G > 0$. Indeed assuming without loss of generality that $f(z)$ vanishes as $|\mathbf{X}| \to \infty$, then $-\int_{\mathrm{X}}(\mathrm{d}^3 f/\mathrm{d}z^3)(\mathrm{d}f/\mathrm{d}z)]\mathrm{d}\mathbf{X} = \int_{\mathrm{X}}(\mathrm{d}^2 f/\mathrm{d}z^2)^2 \mathrm{d}\mathbf{X} > 0$. Notice also that in all problems the λ-parameterization of the macroscopic deformation gradient $\mathbf{F}$ is assumed to produce higher strains for values of λ moving away from λ_{in}, in which case an equation similar to (2.6) holds for β_0 at λ_0. Consequently from $(2.30)_3$, if $\beta_2(\lambda_0) > 0$, λ_2 has the same sign as $\lambda_0 - \lambda_{\mathrm{in}}$, which indicates that, when scale effects are accounted for the critical load, λ_{c} occurs at strains higher than those corresponding to λ_0.

For the case of point-symmetric unit cells discussed in Section 2.4, we have from the vanishing of $\mathscr{M}(\lambda)$ [see (2.27)] that $g_i = 0$ in $(3.5)_2$ which implies that $\overset{1}{\bar{\boldsymbol{\alpha}}}$ also vanishes [see discussion preceding (2.34)], thus simplifying the expression (3.6), for $\beta_2(\lambda_0)$, i.e. when $\mathscr{L}(\lambda, \mathbf{Y}) = \mathscr{L}(\lambda, -\mathbf{Y})$, then

$$\beta_2(\lambda_0) = [\mathscr{N}_{ijspqr}(\lambda_0)\overset{0}{\bar{\alpha}}_i \overset{0}{\bar{\alpha}}_p n_j n_s n_q n_r]G, \tag{3.7}$$

where $G > 0$ is still given by $(3.6)_2$.

A brief justification of the claim made at the end of the previous subsection—on the development of a localized macrofailure mode for those macroscopic strains for which the micro- and macrofailure surfaces coincide—is in order at this point. For the case where a macroscopic loss of ellipticity at λ_0 is the first bifurcation which occurs on the loading path $\mathbf{F}(\lambda)$, the macroscopic force–displacement curve decreases along the bifurcated path as the bifurcation amplitude, say ζ, increases. Without going through a complete post-bifurcation analysis, we remark that the deformation gradient in the neighborhood of λ_0 can be approximated by $F_{ij}(\lambda_0) + \zeta \overset{0}{\bar{\alpha}}_i n_j$ and the average force acting along the characteristic direction is $t \equiv \overset{0}{\bar{\alpha}}_i n_j \int_D \Pi_{ji}$. By recalling from (2.16) the relation between the macroscopic stress and strain rates, one sees that $\mathrm{d}t/\mathrm{d}\zeta = \overset{0}{\bar{\alpha}}_i n_j \mathscr{L}_{ijkl} \overset{0}{\bar{\alpha}}_k n_l$ which vanishes at bifurcation λ_0 and by continuity has to be negative for loading parameters past the bifurcation. For bifurcation problems for

which the total load drops along the bifurcated path, a localization of the buckling pattern develops [see Tvergaard and Needleman (1980)].

In the following section we give examples of macroscopic and microscopic failure surfaces for layered composites under plane strain conditions. In these examples the two failure surfaces can be calculated analytically and the macroscopic moduli $\mathscr{L}(\lambda)$, $\mathscr{M}(\lambda)$, $\mathscr{N}(\lambda)$ are found explicitly.

4. EXAMPLES IN LAYERED COMPOSITES UNDER PLANE STRAIN

The failure surfaces for the periodic composites of infinite extent presented in Section 3 will now be illustrated for the special case of layered materials (laminated composites) under plane strain conditions. The advantage of this illustrative example is that closed form analytical expressions may be obtained for the macroscopic homogenized moduli of all orders. In addition, an exact solution for the microscopic failure surface of laminated periodic composites is possible and the corresponding analyses are briefly outlined in Appendix B.

Two different examples will be discussed here. One involving a layered composite made of two alternating layers of a compressible foam rubber and the other involving a graphite–epoxy composite whose stability under compression has been recently studied experimentally and theoretically by Kyriakides *et al.* (1995). It should be emphasized that the onset of failure load that is of interest here, is a theoretical upper bound for the failure stress of an axially compressed, perfect fiber-reinforced composite. The experimentally measured failure stresses are strongly dependent on the inevitable in practice imperfections, thus requiring a post-bifurcation analysis for the kink band development. The interested reader is referred to Budiansky and Fleck (1993) for an approximate post-bifurcation analysis of this problem or to Kyriakides *et al.* (1995) for a full finite element modeling of their actual (imperfect) composite from the stress-free to a highly localized configuration.

A schematic representation of the laminated composite is shown in Fig. 4. The initial thickness of each fiber and matrix layers are denoted by H_f and H_m, respectively while the initial unit cell thickness is $H = H_f + H_m$. The layered medium deforms in the $X_1 - X_2$ plane, with X_2 the direction perpendicular to lamination. Due to perfect bonding between fiber and matrix layers, kinematics dictate that the axial (X_1-direction) strain is continuous along the interface, while stress equilibrium dictates continuity of the Cauchy stress normal to the interface. It will be further assumed for simplicity that the material properties of each layer are constant throughout the layer and that each layer is orthotropic with respect to the X_1, X_2, X_3 axes.

The loading for the composite consists of a given axial stretch ratio λ_1 and a given normal Cauchy stress σ_2. For this type of loading, and due to the orthotropy and uniform properties of each layer, the resulting stretch ratios and stresses are constant in each layer. Consequently the macroscopic (averaged) stresses and deformation gradients applied to the layered composite are

$$\begin{aligned} &\mathbf{F} = \mathrm{diag}[\lambda_1, \lambda_2], \quad \lambda_1 = \lambda_1^{\mathrm{m}} = \lambda_1^{\mathrm{f}}, \quad \lambda_2 = (\lambda_2^{\mathrm{m}} H_{\mathrm{m}} + \lambda_2^{\mathrm{f}} H_{\mathrm{f}})/H, \\ &\boldsymbol{\sigma} = \mathrm{diag}[\sigma_1, \sigma_2], \quad \sigma_1 = (\sigma_1^{\mathrm{m}} \lambda_2^{\mathrm{m}} H_{\mathrm{m}} + \sigma_1^{\mathrm{f}} \lambda_2^{\mathrm{f}} H_{\mathrm{f}})/H, \quad \sigma_2 = \sigma_2^{\mathrm{m}} = \sigma_2^{\mathrm{f}}, \end{aligned} \tag{4.1}$$

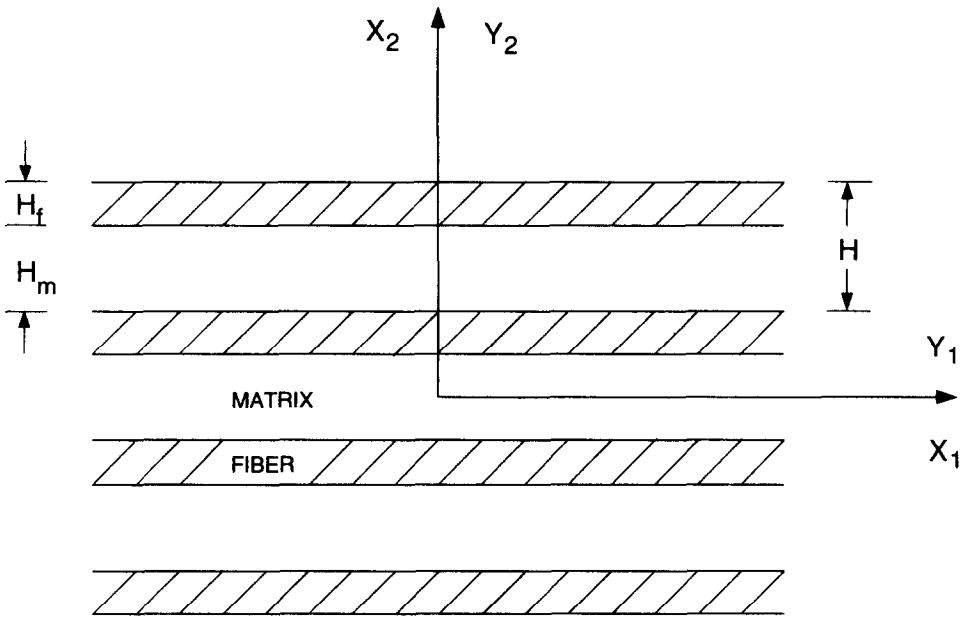

Fig. 4. Schematic representation of a layered composite.

where λ_1^m, λ_2^m and λ_1^f, λ_2^f are the matrix and fiber stretch ratios, respectively, while σ_1^m, σ_2^m and σ_1^f, σ_2^f are the corresponding Cauchy stresses. The scalar loading parameter λ which characterizes the macroscopic loading is the stretch ratio along the fiber direction λ_1, while the dimensionless lateral normal Cauchy stress σ_2/C—C is a conveniently chosen reference stress—is taken proportional to the strain $(\lambda_1 - 1)$ with a coefficient of proportionally s, i.e.

$$\lambda_1 = \lambda, \quad \sigma_2/C = s(\lambda - 1); \quad \lambda_{in} = 1. \tag{4.2}$$

For this parameterization λ_{in}, the value of the load parameter that corresponds to the unloaded configuration, is obviously unity.

Some general remarks are in order at this point about the structure of the incremental moduli $\mathbf{L}(\lambda, \mathbf{X})$ [see definition in (2.1)]. Due to the constant stress and strain fields existing in each layer, the incremental moduli are piecewise constant, i.e. $\mathbf{L}(\lambda, \mathbf{X}) = \mathbf{L}^f(\lambda)$ or $\mathbf{L}^m(\lambda)$ according to whether the material point $\mathbf{X}$ lies in the fiber or in the matrix. The piecewise constant nature of $\mathbf{L}$ simplifies considerably the calculations of the relevant homogenized moduli $\mathscr{L}(\lambda)$, $\mathscr{N}(\lambda)$ [$\mathscr{M}(\lambda) = 0$ for point symmetric unit cells, see Section 2.4].

Additional simplifications result because the incremental moduli $\mathbf{L}$ are piecewise constant. The X_1-independence of the incremental moduli implies the Y_1-independence of the auxiliary Y-periodic functions $\overset{pq}{\boldsymbol{\phi}}(\lambda, \mathbf{Y})$ [defined in $(A.11)_2$] and $\overset{pqr}{\boldsymbol{\psi}}(\lambda, \mathbf{Y})$ [defined in $(A.16)_2$], which are required for the calculation of $\mathscr{L}(\lambda)$ [see (2.18)] and $\mathscr{N}(\lambda)$ [see (2.22)]. The solutions of $(A.11)_2$ and $(A.16)_2$ are straightforward solutions of ordinary differential equations in Y_2 with piecewise constant coefficients. The orthotropy of the incremental moduli simplifies these calculations even further and as a result the

homogenized moduli $\mathscr{L}(\lambda)$, $\mathscr{N}(\lambda)$ have explicit analytical expressions in terms of $\mathbf{L}^{\mathrm{f}}(\lambda)$, $\mathbf{L}^{\mathrm{m}}(\lambda)$, H_{f}/H and H_{m}/H. In the interest of conciseness, the above mentioned derivations as well as the final cumbersome expressions for $\mathscr{L}(\lambda)$ and $\mathscr{N}(\lambda)$ are not recorded in this presentation.

The calculations of the microfailure surfaces for the above described laminated composites, which again require the knowledge of $\mathbf{L}^{\mathrm{f}}(\lambda)$, $\mathbf{L}^{\mathrm{m}}(\lambda)$, H_{f}/H and H_{m}/H, are given in detail in Geymonant *et al.* (1993). It can be shown that the critical load parameter λ_{c}, which corresponds to the onset of first bifurcation $\beta(\lambda_{\mathrm{c}}) = 0$, is found by scanning all the possible dimensionless wavenumbers of the structure only in the X_1-direction. For reasons of completeness of the presentation, a brief outline of all the necessary calculations is presented in Appendix B. In all the calculations reported here, to find the critical load corresponding to the first bifurcation it is sufficient to scan the space $0 \leqslant \omega H \leqslant 20$.

4.1. *Material properties of layered composites*

As mentioned previously, two different types of layered media will be considered in the examples. The first layered medium consists of two alternating layers of compressible foam type rubber described by a Blatz–Ko-type energy density, which for plane strain deformations, i.e. $\lambda_3 = 1$, takes the form [see Blatz and Ko (1962)

$$W = \mu[I_2/I_3 + 2I_3^{1/2} - 5]/2 = \mu[\lambda_1^{-2} + \lambda_2^{-2} + 2\lambda_1\lambda_2 - 4]/2\,;$$
$$I_2 = \tfrac{1}{2}(F_{ij}F_{kl}F_{ij}F_{kl} - F_{ki}F_{kj}F_{li}F_{lj}), \quad I_3 = \det(F_{ki}F_{kj}) \quad i,j,k = 1,2. \tag{4.3}$$

The unique coefficient μ—which is the initial shear modulus of the material—takes different values in the fiber and matrix layers. In all subsequent calculations $\mu_{\mathrm{f}}/\mu_{\mathrm{m}} = 100$, unless explicitly stated otherwise. For any hyperelastic solid the incremental moduli are given by $L_{ijkl} \equiv \partial^2 W/\partial F_{ij}\partial F_{kl}$, with the derivatives evaluated at the deformation of interest, which in the present case is $\mathbf{F} = \mathrm{diag}[\lambda_1, \lambda_2]$. A straightforward calculation gives from (4.3)

$$L_{1111} = 3\mu\lambda_1^{-4}, \quad L_{1122} = L_{2211} = \mu, \quad L_{2222} = 3\mu\lambda_2^{-4},$$
$$L_{1212} = L_{2121} = \mu(\lambda_1\lambda_2)^{-2}, \quad L_{1221} = L_{2112} = \mu(\lambda_1^{-1}\lambda_2^{-3} + \lambda_1^{-3}\lambda_2^{-1} - 1). \tag{4.4}$$

Of interest is also the relation between σ_2 and λ_2 in each layer. From (4.3), and given that for an isotropic hyperelastic material the principal stress σ_2 is given in terms of the stretches λ_i by $\sigma_2 = \lambda_1^{-1}\partial W/\partial\lambda_2$, the relation is found to be

$$\lambda_2 = [\lambda_1(1 - \sigma_2/\mu)]^{-1/3}. \tag{4.5}$$

The second example analyzed is the graphite–peek epoxy composite used in the compressive failure experiments of Kyriakides *et al.* (1995). The required incremental moduli relating $\dot{\Pi}_{ij}$ to $\dot{F}_{kl}$ [see (2.1)] take the form

$$L_{ijkl} = \hat{L}_{ijkl} + \tfrac{1}{2}[\sigma_{ji}\delta_{ik} - \sigma_{jk}\delta_{il} - \sigma_{il}\delta_{jk} - \sigma_{ik}\delta_{jl}] \quad i,j,k,l = 1,3, \tag{4.6}$$

where $\hat{L}_{ijkl}$ are the incremental moduli relating a frame invariant stress-rate measure $(\overset{\nabla}{\boldsymbol{\tau}})$ to its work conjugate strain-rate measure $(\mathbf{D})$. Two different isotropic plasticity

theories—namely the J_2 deformation and the J_2 flow theories, both standard in plasticity calculations—will be employed with both sharing the same experimentally measured uniaxial stress–strain curve. The corresponding expressions for $\hat{L}_{ijkl}$ are

$$\hat{L}_{ijkl} = \frac{\hat{E}}{1+\hat{\nu}}\left[\frac{1}{2}(\delta_{ik}\delta_{jl}+\delta_{il}\delta_{jk})+\frac{\hat{\nu}}{1-2\hat{\nu}}\delta_{ij}\delta_{kl}-\frac{3}{2}\frac{\hat{E}/E_t-1}{\hat{E}/E_t-(1-2\hat{\nu})/3}\frac{\sigma'_{ij}\sigma'_{kl}}{\sigma^2}\right] \quad i,j,k,l=1,3,$$

$$\sigma'_{ij}=\sigma_{ij}-(\sigma_{kk}/3)\delta_{ij}, \quad \sigma^2=(3\sigma'_{ij}\sigma'_{ij}/2), \quad E_t=\mathrm{d}\sigma/\mathrm{d}\varepsilon; \tag{4.7}$$

deformation theory: $\hat{E}=E_s$, $\hat{\nu}=\nu_s$, $E_s=\sigma/\varepsilon$, $(1-2\nu_s)/E_s=(1-2\nu)/E$,
flow theory: $\hat{E}=E$, $\hat{\nu}=\nu$,

where E and ν are the material's Young's modulus and Poisson's ratio while the relation between the equivalent stress σ and the equivalent strain ε is identical to the material's measured uniaxial stress–strain response $\sigma(\varepsilon)$. It should also be mentioned at this point that the incremental moduli in (4.6), (4.7) are given in the updated Lagrangian formulation. Moreover volume change in the material is considered negligible, a fact that permits the identification between Kirchhoff and Cauchy stresses in the current configuration.

The relations between the principal stresses σ_i and the principal strains ε_i for a deformation with fixed principal axes are given in each layer by

$$\varepsilon_i=\ln(\lambda_i)=\frac{1}{E_s}[(1+\nu_s)\sigma_i-\nu_s(\sigma_1+\sigma_2+\sigma_3)]. \tag{4.8}$$

For plane strain experiments $\varepsilon_3=0$ and for a lateral stress $\sigma_2=0$ one obtains from (4.8) and the continuity requirements for $\varepsilon_1=\ln(\lambda_1)$ and σ_2 in (4.1)

$$\varepsilon_1=\frac{(1-\nu_s^2)\sigma}{E_s(1+\nu_s^2-\nu_s)^{1/2}}, \quad \sigma_1=\frac{\sigma}{(1+\nu_s^2-\nu_s)^{1/2}}, \quad \sigma_2=0, \quad \sigma_3=\frac{\nu_s\sigma}{(1+\nu_s^2-\nu_s)^{1/2}}. \tag{4.9}$$

Since ν_s and E_s are known functions of the equivalent stress σ, the equivalent stresses in the matrix and the fiber, σ^m and σ^f, respectively, are found by solving the nonlinear equation $\varepsilon_1^m=\varepsilon_1^f$. The principal stresses in each layer are then completely determined and from (4.7), (4.8) the required incremental moduli are completely specified. Unlike the rubber composite case, for the graphite–epoxy composite the strains at the onset of bifurcation are small (they never exceed 5%) and hence the difference between reference and current configuration can safely be neglected. For this reason, in the presentation of the graphite–epoxy composite results we use the engineering strains $e_i\equiv\lambda_i-1$, instead of the natural (logarithmic) strains $\varepsilon_i\equiv\ln(\lambda_i)$ which are used in the presentation of the results for the rubber composite.

Finally an important general remark is in order at this point. To be meaningful, all the macroscopic and microscopic onset of failure calculations require a stable unit cell according to (A.1). For the layered composites with piecewise constant incremental moduli under consideration, (A.1) implies that the material is locally stable against

localization of deformation in the sense that the strong ellipticity condition holds at all times for both fiber and matrix, i.e. that

$$L_{ijkl}(\lambda)\alpha_i n_j \alpha_k n_l > 0, \quad \|\boldsymbol{\alpha}\| = \|\mathbf{n}\| = 1, \tag{4.10}$$

where $\mathbf{L} = \mathbf{L}^{\mathrm{f}}$ or $\mathbf{L} = \mathbf{L}^{\mathrm{m}}$. The above local stability condition for each constituent of the composite is checked for each state of deformation. Unless otherwise stated, all the micro- and macrofailure surfaces reported below occur at stress states λ for which (4.10) is satisfied.

4.2. *Results and discussion*

The macro- and microfailure surfaces for the stratified composites made of compressible rubber are given in Fig. 5. The results are presented in principal macroscopic strain space $(\varepsilon_1 - \varepsilon_2)$, with the solid line marking the onset of the first bifurcation (microfailure) and the dashed line marking the onset of the loss of ellipticity for the homogenized composite (macrofailure). All calculations correspond to an initial fiber-to-matrix stiffness ratio $\mu_{\mathrm{f}}/\mu_{\mathrm{m}} = 100$. The stretch ratios investigated are in the interval $0.5 < \lambda_1, \lambda_2 < 2.5$. The reference stress used in the definition of the lateral stress-rate parameter s in (4.2) is taken for all the calculations for rubber composites to be $C = \mu_{\mathrm{m}}$.

The results in Fig. 5(a) correspond to a high fiber volume fraction $H_{\mathrm{f}}/H = 0.25$ (thick fiber). For the case of axial compression along the fibers ($\varepsilon_1 < 0$), the first bifurcation mode of the composite has an infinite wavelength, and hence the micro- and macrofailure curves coincide. Moreover, for all the points on the macrofailure surface $\beta_2 > 0$. For the case of axial tension along the fiber direction ($\varepsilon_1 > 0$), the first bifurcation mode of the infinite medium has a finite wavelength, and hence microfailure occurs prior to the macrofailure. Moreover, all points on the macrofailure surface have $\beta_2 < 0$. The results of the higher order gradient calculations are thus in agreement with the conclusions in Section 3, according to which $\beta_2 < 0$ indicates a microfailure prior to the macroscopic one, while $\beta_2 > 0$ indicates that a first bifurcation instability coincident with macrofailure is a possibility. The triangle ($\triangle$) which appears at the endpoint ($\varepsilon_2 \approx -0.5$) of the axial tension macrofailure curve ($\varepsilon_1 > 0$) indicates that bifurcation on the unit cell is possible [$(4.10)_1$ no longer holds], and hence the curve is discontinued at this point.

The results in Fig. 5(b) correspond to a low fiber volume fraction $H_{\mathrm{f}}/H = 0.05$ (thin fiber). For either axial compression or tension along the fibers, the first bifurcation instability of the infinite medium always has a finite wavelength, and hence microfailure occurs prior to the macrofailure. All points on the macrofailure surface have $\beta_2 < 0$, thus confirming in this case the presence of a microfailure prior to reaching the strain state at macrofailure. The same comment as in the preceding paragraph applies regarding the appearance of the triangle ($\triangle$).

The results in Fig. 5(c) correspond to an intermediate fiber volume fraction $H_{\mathrm{f}}/H = 0.1$. Notice that in the case of axial compression along the fibers ($\varepsilon_1 < 0$), the micro- and macrofailure surfaces coincide only for high lateral compression ($\varepsilon_2 < -0.7$), while the microfailure occurs prior to the macro one for ($\varepsilon_2 > -0.7$). The distance between the two failure surfaces in compression is so small that it does

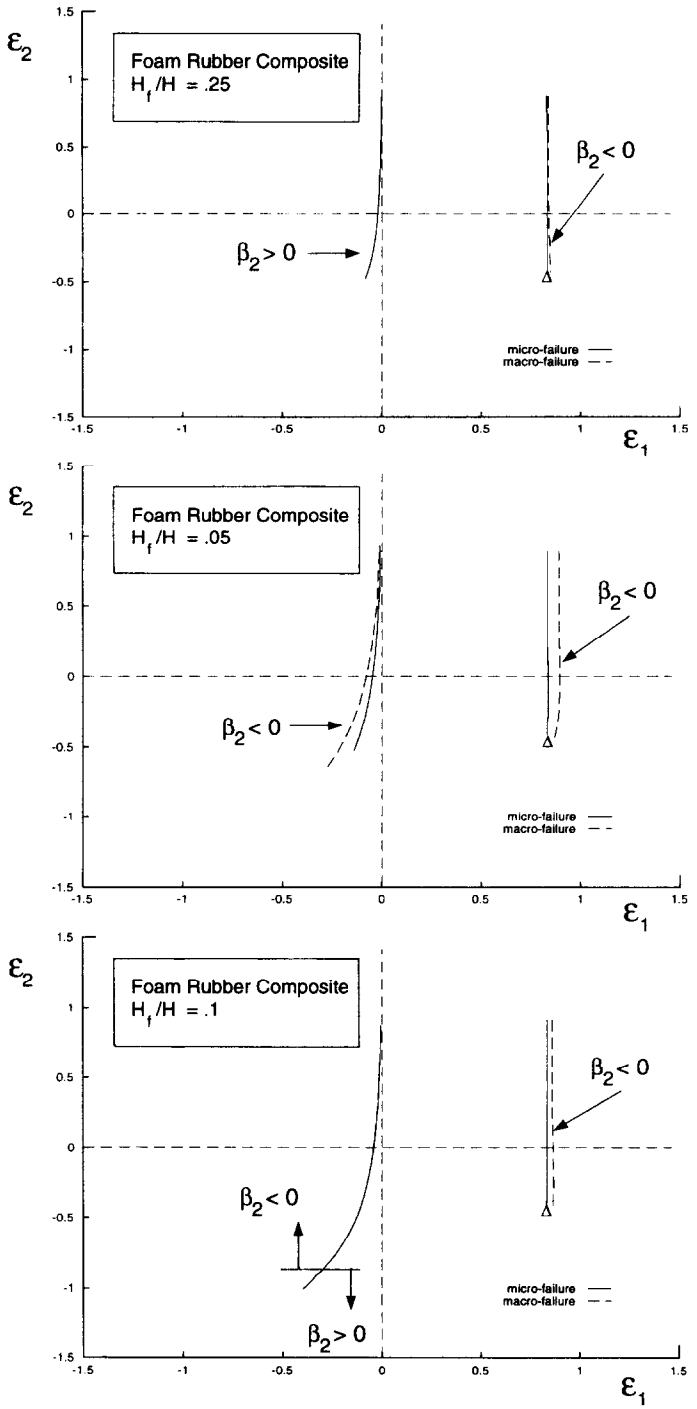

Fig. 5. Micro- and macrofailure surfaces for a layered rubber composite, which is subjected to a state of macroscopic finite biaxial strain ε_1, ε_2, are calculated for three different fiber volume fractions. Results for a thick fiber are depicted in (a), for a thin fiber in (b) and for a medium thickness fiber in (c). Notice that the criterion based on the higher order average moduli ($\beta_2 < 0$), is necessary and sufficient for the separation of the two failure surfaces.

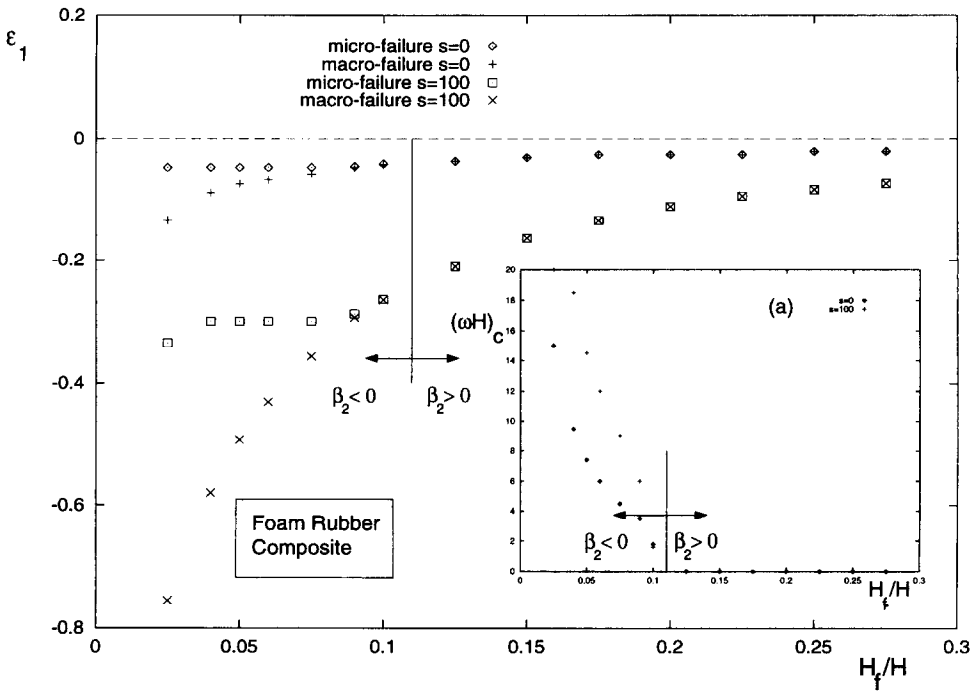

Fig. 6. Micro- and macrofailure natural strain ε_1 for a layered rubber composite as a function of fiber volume fraction H_f/H. For fiber thicknesses exceeding a threshold value, the two failure strains coincide and the criterion based on the higher order average moduli ($\beta_2 < 0$), is necessary and sufficient for the separation of the two failure surfaces. The dimensionless axial critical wavenumber $(\omega H)_c$ as a function of the fiber volume fraction H_f/H is given in insert (a). Notice the stabilization effect of the lateral compressive stresses ($s \neq 0$), which lead to higher critical strains.

not show well in the scale of the present graph. The results in tension are similar to the previous two cases, with the macrofailure always occurring after the microfailure. Consistent with the two previous cases, $\beta_2 < 0$ for the points where the microfailure occurs prior to the macro one and $\beta_2 > 0$ when the two failure surfaces coincide. The significance of the triangle ($\triangle$) is as described above.

As seen from the above calculations, composites with low fiber volume fraction have a first instability mode with a finite wavelength, while as the fiber volume fraction increases, the first instability mode has an infinite wavelength. The dependence of the dimensionless critical wavenumber in the axial direction $(\omega H)_c$ on the fiber volume fraction H_f/H is depicted in the insert of Fig. 6. Data points denoted by $\diamond$ correspond to the absence of lateral stress $s = 0$ while data points denoted by $+$ correspond to a lateral stress rate parameter $s = 100$ [recall the definition for s in (4.2) $\sigma_2/C = s(\lambda - 1)$]. Note the rapid increase of $(\omega H)_c$ as fiber thicknesses decrease below the approximate threshold value $H_f/H = 0.1$, indicating the wavelength of the first bifurcation eigenmode decreases rapidly for thinner fibers. For fiber thicknesses $1 > H_f/H > 0.1$ the macro- and microinstabilities coincide and $(\omega H)_c = 0$. The critical strains ε_1, corresponding to the micro- and macrofailures of these composites are plotted against the fiber volume fraction H_f/H in Fig. 6. In the absence of lateral stress $s = 0$, the

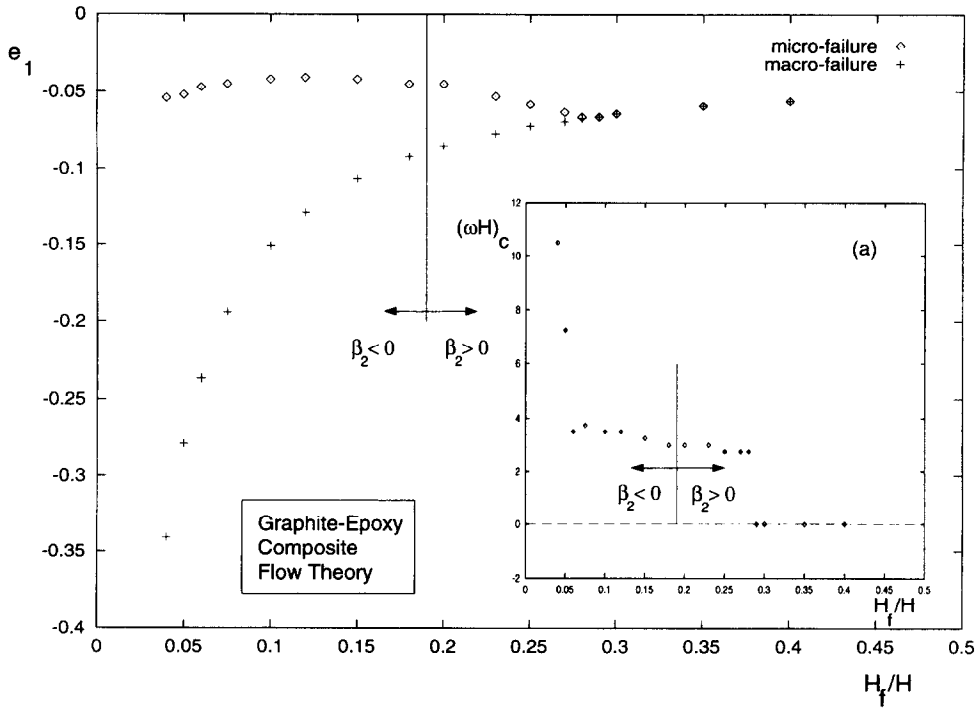

Fig. 7. Micro- and macrofailure engineering strain e_1 for an axially compressed, layered graphite–epoxy composite as a function of fiber volume fraction H_f/H, based on deformation theory of plasticity. For fiber thicknesses exceeding a threshold value, the two failure strains coincide and the criterion based on the higher order average moduli ($\beta_2 < 0$), is sufficient but not necessary for the separation of the two failure surfaces. The dimensionless axial critical wavenumber $(\omega H)_c$ as a function of the fiber volume fraction H_f/H is given in insert (a).

microfailure points for a given fiber thickness are denoted by $\diamond$ and their corresponding macrofailure points are denoted by $+$. For the case of a lateral stress rate parameter $s = 100$, the microfailure points are denoted by $\square$ and their corresponding macrofailure points are denoted by $\times$. Notice the stabilizing effect of lateral compression ($s \neq 0$), leading to higher critical strains. As expected from Fig. 6(a), the micro- and macrofailure surfaces coincide for fiber thicknesses $1 > H_f/H > 0.1$ and are distinct for $0 < H_f \leqslant 0.1$ (the distance between micro- and macrofailure strains is so small that it does not show well in the scale of the graph). Consistent with all the previous calculations, $\beta_2 < 0$ for the points where the microfailure occurs prior to the macro one and $\beta_2 > 0$ when the two failure surfaces coincide. Thus for the stratified media made of Blatz–Ko type rubber, the higher order gradient criterion, which gives the sign of β_2, is a reliable indicator for both the coincidence and distinctness of the micro- and macrofailure surfaces of the infinite composite.

The calculations of the micro- and macrofailure for the graphite–epoxy composite are limited to uniaxial compression along the fiber direction and are done in the absence of lateral stress, in conformity with the experiments of Kyriakides *et al.* (1995). The present calculations extend over the entire range of possible fiber volume fractions, while the experimental results reported in the above paper were obtained for $H_f/H = 0.6$. The deformation theory results are presented in Fig. 7. More specifi-

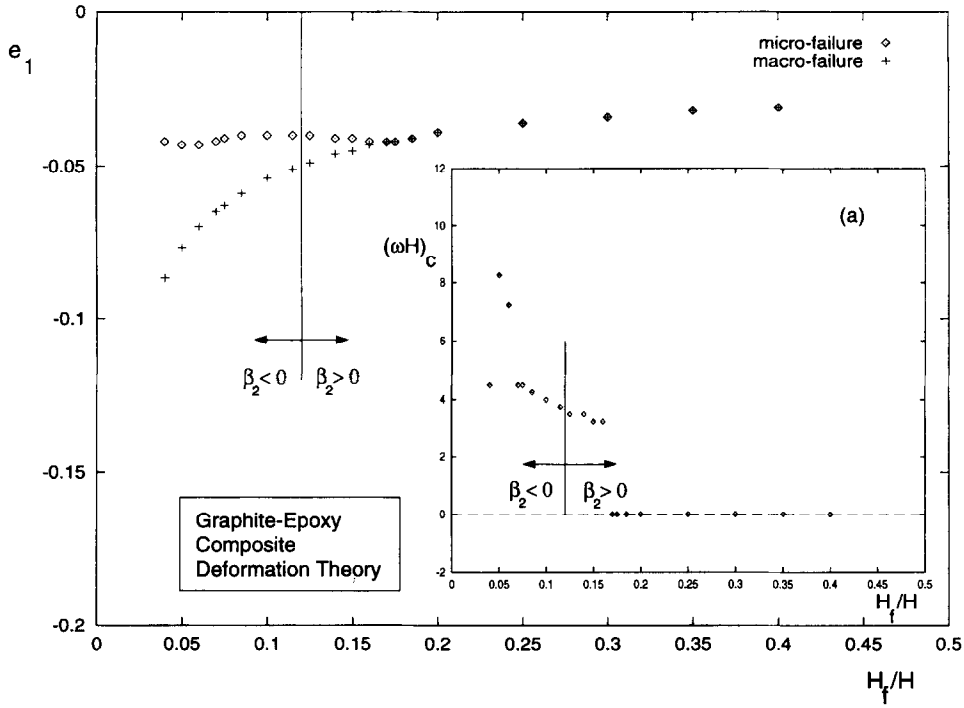

Fig. 8. Micro- and macrofailure engineering strain e_1 for an axially compressed, layered graphite–epoxy composite as a function of fiber volume fraction H_f/H, based on flow theory of plasticity. For fiber thicknesses exceeding a threshold value, the two failure strains coincide and the criterion based on the higher order average moduli ($\beta_2 < 0$), is sufficient but not necessary for the separation of the two failure surfaces. The dimensionless axial critical wavenumber $(\omega H)_c$ as a function of the fiber volume fraction H_f/H is given in insert (a). Notice that the critical strain predictions of the flow theory are higher than those of the deformation theory in Fig. 7.

cally, the dependence of the dimensionless critical wavenumber in the axial direction $(\omega H)_c$ on the fiber volume fraction H_f/H is depicted in the insert of Fig. 7. Notice that the approximate threshold dimensionless fiber thickness above which the macro- and microinstabilities coincide is $H_f/H = 0.29$. Also notice the rapid increase of $(\omega H)_c$ for dimensionless fiber thicknesses below $H_f/H = 0.05$ indicating the wavelength of the first bifurcation eigenmode decreases rapidly for thinner fibers. The corresponding critical axial engineering strains e_1 for the micro- (denoted by $\diamond$) and the macrofailure (denoted by $+$) are depicted in Fig. 7. As discussed in Section 3, $\beta_2 < 0$ is simply a sufficient criterion for the presence of a microfailure prior to a macrofailure (in contrast to the rubber composite results in Fig. 6, where the sign of β_2 is a reliable indicator for both the coincidence and distinctness of the micro- and macrofailure surfaces of the infinite composite). Here the higher order gradient criterion for detection of a local failure prior to global failure, i.e. $\beta_2 < 0$, gives only a portion of the entire fiber thickness range for which microfailure precedes macrofailure.

The calculations in Fig. 8 are a repetition of the ones in Fig. 7 but correspond to

the flow theory version of the graphite–epoxy composite. As expected, one difference in the results is the flow theory's consistent increase of critical strains for the onset of micro- and macroinstabilities of the composite. Notice also that the threshold value of the fiber thickness, above which the micro- and macrofailure surfaces coincide, is here much smaller, approximately $H_f/H = 0.17$. The erratic behavior of $(\omega H)_c$ for dimensionless fiber thickness $H_f/H < 0.05$ is due to the competition between nearly simultaneous eigenmodes of different (finite) wavelengths. The same comments as in the previous paragraph apply regarding the higher order gradient criterion's ability to determine only a portion of the entire region for which microfailure precedes macrofailure.

The experiments by Kyriakides *et al.* (1995) are for $H_f/H = 0.6$ where the failure mode observed was a kink-band type instability. This is in agreement with Figs 7 and 8, as macrofailure is predicted for this fiber thickness ratio (see Section 3.1). It is worth noticing that due to the presence of imperfections, the post-buckling behavior of the graphite–epoxy composite produced compressive critical strains of the order of 1%, considerably lower than the onset of instability strains of just below 4% predicted by the deformation theory.

5. CONCLUDING REMARKS

The issue of incorporating scale size information in studying the stability and failure of microstructured solids has attracted considerable interest in recent years. One popular approach to model scale size effects is through the inclusion of higher order gradients in the kinematical description or in the evolution laws for the internal variables. Although many micromechanical justifications for these types of models have been proposed, the consistent derivation of these higher order gradient models from the properties of the underlying microstructure is still an open problem.

The present work is a continuation of some recent efforts by the authors to obtain scale size information in the continuum description of solids with periodic microstructures. Unlike the previous results which concentrated on finding the macroscopic behavior of discrete elastic media under finite average strains, this work investigates the stability of rate-independent elastoplastic continua with periodic microstructures. Although an overall continuum description of the microstructured medium for arbitrary macroscopic states of deformation is not feasible, the study of the onset of instability in terms of the scale size parameter ε is possible by means of a multiple scales asymptotic expansion for the lowest critical load and corresponding mode. It is found that the zeroth order ε terms in these expansions depend on the standard (first order gradient) macroscopic moduli tensor, while all the higher order ε terms require the determination of higher order gradient macroscopic moduli. These macroscopic moduli, which are calculated by solving appropriate boundary value problems on the unit cell, relate the macroscopic (unit cell average) stress rate increment to the macroscopic displacement rate gradients.

Motivated by failure problems in ductile composites under essentially compressive macroscopic stresses, we present a novel application of the proposed general theory, which involves the investigation of failure surfaces in periodic solids of infinite extent.

For these solids one can define in macroscopic strain space a microscopic and a macroscopic failure surface. The determination of the macrofailure surface, which requires the calculation of the standard macroscopic moduli tensor, is considerably easier than the determination of the microfailure surface. In addition, the regions where the two surfaces coincide is of significant practical interest, for a macroscopic localization mode of deformation appears in the post-bifurcation regime. The prediction of these coincidence zones is based on a necessary criterion which depends on the higher order gradient macroscopic moduli. The above mentioned necessary criterion for the coincidence of the micro- and macrofailure surfaces is verified from detailed calculations in layered composites.

Some additional comments are in order at this point about the proposed failure surfaces concept for ductile periodic (or nearly periodic) solids which are subjected mainly to compressive stresses. The proposed surfaces are calculated for perfect microstructures and thus provide upper bounds for the failure loads of the composite [imperfections in the geometry and properties of the microstructure result in failure surfaces nested inside their counterparts for the perfect case, see Schraad and Triantafyllidis (1996)]. We should also keep in mind that the proposed failure surface approach gives us the possibility of investigating all possible stress tensor orientations, a task which presents considerable experimental difficulties. Most experimental failure studies in periodic media (fiber reinforced, honeycombs, etc.) are done for a fixed load path (usually uniaxial) and a fixed loading direction with respect to the microstructure. Calculations under way for certain periodic composites (current work for honeycomb composites by Triantafyllidis and Schraad—unpublished work) show extreme sensitivity of the failure surfaces to the stress tensor direction. Moreover, given that the microfailure surface calculations are considerably more computational intensive than their macrofailure surface counterparts, the proposed higher order gradient moduli criterion is, in our opinion, a valuable modeling tool. It helps in finding stress states that lead to possible localization of deformation, it can aid in the detection of the most "dangerous" stress states and hence it can help us to design appropriate microstructures.

There are a number of further applications for the higher order gradient macroscopic moduli derived by the present approach. One such case is the study of the post-bifurcation localization in periodic composites and layered media, for the case where the localized zone size is several times larger than the thickness of the unit cell. For this case, a continuum approach for the solution of the overall boundary value problem is the most efficient to predict the spatial development of the localized deformation zones. This direction of work seems to be the next logical step in applying the results of the present investigation to engineering problems involving the failure of microstructured solids.

ACKNOWLEDGEMENTS

The present work was partially funded by Grant DOD-G-F49620-94-1-0402 from the AFOSR, the support of which is gratefully acknowledged. The authors also wish to thank Dr Owen Richmond of ALCOA Research Labs for his continuing encouragement, support and

long discussions on the subject on non-local theories in solids over the past four years. We also acknowledge the help of Professor Stelios Kyriakides who made available his experimental data to us and helped with many insightful discussions on the compressive failure of laminated composites.

REFERENCES

Abeyaratne, R. and Triantafyllidis, N. (1984) An investigation of localization in a porous elastic material using homogenization theory. *J. Appl. Mech.* **51,** 481–486.

Aifantis, E. C. (1984) On the microstructural origin of certain inelastic models. *J. Engng Mater. Technol.* **106,** 326–330.

Aifantis, E. C. (1987) The physics of plastic deformation. *Int. J. Plasticity* **3,** 211–247.

Bardenhagen, S. G. and Triantafyllidis, N. (1994) Derivation of higher order gradient continuum theories in 2,3-D non-linear elasticity from periodic lattice models. *J. Mech. Phys. Solids* **42,** 111–139.

Benallal, A. and Tvergaard, V. (1995) Nonlocal continuum effects on bifurcation in the plane strain tension-compression test. *J. Mech. Phys. Solids* **43,** 741–770.

Blatz, P. J. and Ko, W. L. (1962) Application of finite elastic theory to the deformation of rubbery materials. *Trans. Soc. Rheol.* **6,** 223–251.

Budiansky, B. and Fleck, N. A. (1993) Compressive failure of fiber composites. *J. Mech. Phys. Solids* **41,** 183–211.

Fleck, N. A. and Hutchinson, J. W. (1993) A phenomenological theory of strain gradient plasticity. *J. Mech. Phys. Solids* **41,** 1825–1857.

Geymonant, G., Müller, S. and Triantafyllidis, N. (1993) Homogenization of nonlinearly elastic materials, microscopic bifurcation and macroscopic loss of rank-one convexity. *Arch. Rat. Mech. Anal.* **122,** 231–290.

Gurson, A. L. (1977) Continuum theory of ductile rupture by void nucleation and growth—I. *J. Engng Mater. Technol.* **99,** 2–15.

Hill, R. (1958) A general theory of uniqueness and stability in elastic-plastic solids. *J. Mech. Phys. Solids* **6,** 236–249.

Kyriakides, S., Arsecularatne, R., Perry, E. J. and Liechti, K. M. (1995) On the compressive failure of fiber reinforced composites. *Int. J. Sol. Structure* **32,** 689–738.

Leroy, Y. M. and Molinari, A. (1993) Spatial patterns and size effects in shear zones: A hyperelastic model with higher-order gradients. *J. Mech. Phys. Solids* **41,** 631–664.

Mindlin, R. D. (1964) Micro-structure in linear elasticity. *Arch. Rat. Mech. Anal.* **16,** 51–78.

Muhlhaus, H. B. and Aifantis, E. C. (1991) A general theory of uniqueness and stability in elastic–plastic solids. *J. Mech. Phys. Solids* **6,** 236–249.

Müller, S. (1987) Homogenization of nonconvex integral functionals and cellular elastic materials. *Arch. Rat. Mech. Anal.* **99,** 189–212.

Nguyen, Q. S. and Triantafyllidis, N. (1989) Plastic bifurcation and postbifurcation for generalized standard continua. *J. Mech. Phys. Solids* **37,** 545–566.

Sanchez-Palencia, E. (1974) Comportements local et macroscopique d'un type de milieux physiques hétérogènes. *Int. J. Engng Sci.* **12,** 331–351.

Schraad, M. W. and Triantafyllidis, N. (1996) Scale size effects in periodic and nearly periodic media—II. Failure mechanisms, submitted for publication.

Triantafyllidis, M and Aifantis, E. C. (1986) A gradient approach to localization of deformation. I—Hyperelastic materials. *J. Elasticity* **16,** 225–237.

Triantafyllidis, N. and Maker, B. N. (1985) On the comparison between microscopic and macroscopic instability mechanisms in a class of fiber-reinforced composites. *J. Appl. Mech.* **52,** 794–800.

Triantafyllidis, N. and Bardenhagen, S. G. (1993) On higher order gradient continuum theories in 1-D nonlinear elasticity. Derivation from and comparison to the corresponding discrete models. *J. Elasticity* **33,** 259–293.

Tvergaard, V. and Needleman, A. (1980) On the localization of buckling patterns. *J. Appl. Mech.* **47**, 613–619.

Van Der Waals, J. D. (1893) The thermodynamic theory of capillarity under the hypothesis of a continuous variation of density (in Dutch). *Verhandel. Konink. Akad. Weten. Amsterdam* (sec. 1) **1**.

APPENDIX A: ASYMPTOTIC ANALYSIS FOR MINIMUM EIGENVALUE AND EIGENMODE

In this appendix the details of the derivation of the variational statements presented in Section 2.2 are presented. Recall that a function defined on V is termed Y-periodic if it is periodic and assumes the same values on opposite faces of the parallelepiped unit cell. In the microscopic coordinates $\mathbf{Y} = \mathbf{X}/\varepsilon$ the unit cell is denoted by D and its boundary by ∂D.

Some intermediate results, which will be used repeatedly in the course of the ensuing asymptotic calculations, are first recorded. Recall the assumption, made in the beginning of Section 2, that the first critical mode is global in nature, i.e. that its characteristic wavelength is much larger than the unit cell size. This assumption implies that for any load λ of interest the solid is locally stable, i.e. no bifurcation instability of the unit cell is possible

$$\overset{\min}{\boldsymbol{\phi}} \int_D L_{ijkl}(\lambda, \mathbf{Y}) \frac{\partial \phi_i}{\partial Y_j} \frac{\partial \phi_k}{\partial Y_l} \mathrm{d}\mathbf{Y} > 0; \quad \boldsymbol{\phi}(\mathbf{Y}) \text{ is } Y\text{-periodic}, \quad \|\boldsymbol{\phi}\|^2 = \phi_i \phi_i = 1, \quad \int_D \boldsymbol{\phi} \mathrm{d}\mathbf{Y} = 0. \tag{A.1}$$

As long as $\beta(\lambda) > 0$, the unit cell stability condition (A.1) follows from (2.3), as a special case of the global stability of the entire solid. The additional information in (A.1) is that it holds for any load level λ, even the ones in the neighborhood of λ_c. As a result of (A.1) the following linear boundary value problem has a unique Y-periodic solution $\mathbf{f}(\mathbf{Y})$, whose average vanishes over the unit cell

$$\int_D L_{ijkl}(\lambda, \mathbf{Y}) \frac{\partial f_k}{\partial Y_l} \frac{\partial \phi_i}{\partial Y_j} \mathrm{d}\mathbf{Y} = \int_D g_i \phi_i \mathrm{d}\mathbf{Y}, \quad \text{for all } Y\text{-periodic } \boldsymbol{\phi}(\mathbf{Y}), \tag{A.2}$$

where $\mathbf{g}(\mathbf{Y})$ is given Y-periodic function whose average also vanishes over the unit cell.

An additional simple result that will prove very useful in the sequel is that the average over the unit cell of the gradient of any Y-periodic function $\boldsymbol{\phi}(\mathbf{Y})$ vanishes, i.e.

$$\int_D \frac{\partial \phi_i}{\partial Y_j} \mathrm{d}\mathbf{Y} = \int_{\partial D} \phi_i n_i \mathrm{d}S = 0, \tag{A.3}$$

since the outward normal components n_i have opposite values at opposite faces of the unit cell while ϕ_i takes the same values on opposite faces.

All the ingredients are now in place to find β_i and $\overset{i}{\mathbf{v}}$. The starting point of the corresponding calculations is the variational equation that defines β and $\mathbf{v}$ in $(2.4)_1$. Using the chain rule of differentiation to replace $\mathrm{d}/\mathrm{d}X_i$ by $\partial/\partial X_i + \varepsilon^{-1}\partial/\partial Y_i$ in conjunction with (2.11), (2.12), variational equation $(2.4)_1$ reads

$$\int_{\mathbf{X}} \Bigg[\int_D \Bigg[L_{ijkl}(\lambda, \mathbf{Y}) \left(\frac{\partial}{\partial X_l} + \frac{1}{\varepsilon} \frac{\partial}{\partial Y_l} \right) \left[\overset{0}{v}_k + \varepsilon \overset{1}{v}_k + \cdots \right] \left(\frac{\partial \delta v_i}{\partial X_j} + \frac{1}{\varepsilon} \frac{\partial \delta v_i}{\partial Y_j} \right) - (\beta_0(\lambda) + \varepsilon \beta_1(\lambda) + \cdots)(\overset{0}{v}_i + \varepsilon \overset{1}{v}_i + \cdots) \delta v_i \Bigg\} \mathrm{d}\mathbf{Y} \Bigg] \mathrm{d}\mathbf{X} = 0. \tag{A.4}$$

Collecting the lowest order ε terms in (A.4) gives

$$O(\varepsilon^{-2}): \quad \int_{\mathbf{X}}\left[\int_{D}\left\{L_{ijkl}(\lambda,\mathbf{Y})\frac{\partial \overset{0}{v}_k}{\partial Y_l}\frac{\partial \delta v_i}{\partial Y_j}\right\}\mathrm{d}\mathbf{Y}\right]\mathrm{d}\mathbf{X}=0. \tag{A.5}$$

Rewriting the integrand of (A.5) gives

$$\int_{\mathbf{X}}\left[\int_{D}\left\{\frac{\partial}{\partial Y_j}\left[L_{ijkl}(\lambda,\mathbf{Y})\frac{\partial \overset{0}{v}_k}{\partial Y_l}\delta v_i\right]-\frac{\partial}{\partial Y_j}\left[L_{ijkl}(\lambda,\mathbf{Y})\frac{\partial \overset{0}{v}_k}{\partial Y_l}\right]\delta v_i\right\}\mathrm{d}\mathbf{Y}\right]\mathrm{d}\mathbf{X}=0. \tag{A.6}$$

Integration over D of the first term in (A.6) and the Y-periodicity of $\mathbf{L}$, $\overset{0}{\mathbf{v}}$ and $\delta\mathbf{v}$ imply, in view of (A.3), a vanishing contribution of this term. From the second term in (A.6) and the arbitrariness of $\delta\mathbf{v}$ we deduce

$$\frac{\partial}{\partial Y_j}\left[L_{ijkl}(\lambda,\mathbf{Y})\frac{\partial \overset{0}{v}_k}{\partial Y_l}\right]=0. \tag{A.7}$$

The above equation is the Euler–Lagrange equation that corresponds to (A.2) in which the right hand side term is $\mathbf{g}=\mathbf{0}$. Consequently, the only possible Y-periodic solution $\overset{0}{v}_k$ of (A.7) is a constant with respect to $\mathbf{Y}$, i.e.

$$\overset{0}{v}_i(\lambda,\mathbf{X},\mathbf{Y})=\overset{0}{\bar{v}}_i(\lambda,\mathbf{X}). \tag{A.8}$$

The next order of ε term in the expansion of (A.4), making use of (A.8), is

$$O(\varepsilon^{-1}): \quad \int_{\mathbf{X}}\left[\int_{D}\left\{L_{ijkl}(\lambda,\mathbf{Y})\left(\frac{\partial \overset{0}{v}_k}{\partial X_l}+\frac{\partial \overset{1}{v}_k}{\partial Y_l}\right)\frac{\partial \delta v_i}{\partial Y_j}\right\}\mathrm{d}\mathbf{Y}\right]\mathrm{d}\mathbf{X}=0. \tag{A.9}$$

Following the same steps as for (A.5) of rewriting the integrand in (A.9) and subsequently exploiting (A.3) as well as the arbitrariness of $\delta\mathbf{v}$, the following differential equation is obtained for $\overset{1}{\mathbf{v}}$

$$\frac{\partial}{\partial Y_j}\left[L_{ijkl}(\lambda,\mathbf{Y})\frac{\partial \overset{1}{v}_k}{\partial Y_l}\right]=-\frac{\partial}{\partial Y_j}\left[L_{ijkl}(\lambda,\mathbf{Y})\frac{\partial \overset{0}{\bar{v}}_k}{\partial X_l}\right]. \tag{A.10}$$

In view of (A.3), the right hand side of (A.10) is a Y-periodic function whose average vanishes over the unit cell. Consequently, and according to (A.2), $\overset{1}{\mathbf{v}}$ can be written as

$$\overset{1}{v}_i(\lambda,\mathbf{X},\mathbf{Y})=\overset{pq}{\phi}_i(\lambda,\mathbf{Y})\frac{\partial \overset{0}{\bar{v}}_p}{\partial X_q}(\lambda,\mathbf{X})+\overset{1}{\bar{v}}_i(\lambda,\mathbf{X}), \tag{A.11}$$

where

$$\frac{\partial}{\partial Y_j}\left[L_{ijkl}(\lambda,\mathbf{Y})\frac{\partial \overset{pq}{\phi}_k}{\partial Y_l}\right]=-\frac{\partial}{\partial Y_j}\left[L_{ijpq}(\lambda,\mathbf{Y})\right]; \quad \overset{pq}{\boldsymbol{\phi}} \text{ is } Y\text{-periodic}, \quad \int_{D}\overset{pq}{\boldsymbol{\phi}}\,\mathrm{d}\mathbf{Y}=0. \tag{A.11}_2$$

Notice that the above defined functions $\overset{pq}{\boldsymbol{\phi}}$ are the unique Y-periodic solutions of (A.11)$_2$ with zero average over the unit cell, according to (A.2). A simple superposition argument shows that the first term for $\overset{1}{\mathbf{v}}$ is the corresponding Y-periodic solution of (A.10) with zero average over the unit cell. The constant in $\mathbf{Y}$ term $\overset{1}{\mathbf{v}}$ appearing in (A.11)$_1$ is needed since, according to the remarks made about $\overset{i}{\mathbf{v}}$ in (2.12), the average of $\overset{i}{\mathbf{v}}$ over the unit cell is in general a function of the macroscopic variable $\mathbf{X}$.

The next higher order $O(\varepsilon^0)$ term in the expansion of (A.9) is

$$O(\varepsilon^0): \quad \int_{\mathbf{X}}\Bigg[\int_D \Bigg\{L_{ijkl}(\lambda,\mathbf{Y})\left(\frac{\partial \overset{0}{v}_k}{\partial X_l}+\frac{\partial \overset{1}{v}_k}{\partial Y_l}\right)\frac{\partial \delta v_i}{\partial X_j}+L_{ijkl}(\lambda,\mathbf{Y})\left(\frac{\partial \overset{1}{v}_k}{\partial X_l}+\frac{\partial \overset{2}{v}_k}{\partial Y_l}\right)\frac{\partial \delta v_i}{\partial Y_j} - \beta_0(\lambda)\overset{0}{v}_i\delta v_i\Bigg\}\mathrm{d}\mathbf{Y}\Bigg]\mathrm{d}\mathbf{X}=0. \quad \text{(A.12)}$$

By selecting a $\delta\mathbf{v}$ independent of $\mathbf{Y}$, namely $\delta\mathbf{v}=\delta\bar{\mathbf{v}}(\mathbf{X})$, and recalling (A.8), (A.12) yields with the help of (A.11) the following variational statement for $\beta_0(\lambda)$ and the corresponding eigenmode $\overset{0}{\bar{\mathbf{v}}}(\lambda,\mathbf{X})$

$$\int_{\mathbf{X}}\left[\mathscr{L}_{ijpq}(\lambda)\frac{\partial \overset{0}{\bar{v}}_p}{\partial X_q}\frac{\partial \delta\bar{v}_i}{\partial X_j}-\beta_0(\lambda)\overset{0}{\bar{v}}_i\delta\bar{v}_i\right]\mathrm{d}\mathbf{X}=0, \quad \text{(A.13)}_1$$

$$\mathscr{L}_{ijpq}(\lambda)\equiv\frac{1}{\mathrm{vol}\,D}\int_D\left[L_{ijkl}(\lambda,\mathbf{Y})\left(\delta_{pk}\delta_{ql}+\frac{\partial \overset{pq}{\phi}_k}{\partial Y_l}\right)\right]\mathrm{d}\mathbf{Y}. \quad \text{(A.13)}_2$$

In analogy to the analysis of (A.9), which provided the Y-dependence of $\overset{1}{\mathbf{v}}$, from (A.12) one can deduce the Y-dependence of $\overset{2}{\mathbf{v}}$. By appropriately rewriting the integrand in (A.12) and subsequently exploiting (A.3) one obtains

$$\int_{\mathbf{X}}\left[\frac{\partial}{\partial X_j}\left(\int_D\left\{L_{ijkl}(\lambda,\mathbf{Y})\left(\frac{\partial \overset{0}{v}_k}{\partial X_l}+\frac{\partial \overset{1}{v}_k}{\partial Y_l}\right)\delta v_i\right\}\mathrm{d}\mathbf{Y}\right)\right]\mathrm{d}\mathbf{X}-\int_{\mathbf{X}}\Bigg[\int_D\Bigg\{\frac{\partial}{\partial X_j}\left[L_{ijkl}(\lambda,\mathbf{Y})\left(\frac{\partial \overset{0}{v}_k}{\partial X_l}+\frac{\partial \overset{1}{v}_k}{\partial Y_l}\right)\right]+\frac{\partial}{\partial Y_j}\left[L_{ijkl}(\lambda,\mathbf{Y})\left(\frac{\partial \overset{1}{v}_k}{\partial X_l}+\frac{\partial \overset{2}{v}_k}{\partial Y_l}\right)\right]+\beta_0(\lambda)\overset{0}{v}_i\Bigg\}\delta v_i\mathrm{d}\mathbf{Y}\Bigg]\mathrm{d}\mathbf{X}=0.$$

In view of the arbitrariness of δv_i, and with the help of the Euler–Lagrange equation corresponding to (A.13), plus the expressions for $\overset{0}{\mathbf{v}},\overset{1}{\mathbf{v}}$ in (A.8), (A.11), one obtains from (A.14) the following differential equation for $\overset{2}{\mathbf{v}}$

$$\frac{\partial}{\partial Y_j}\left[L_{ijkl}(\lambda,\mathbf{Y})\frac{\partial \overset{2}{v}_k}{\partial Y_l}\right]=\Bigg\{\left[\mathscr{L}_{ijpq}(\lambda)-L_{ijkl}(\lambda,\mathbf{Y})\left(\delta_{pk}\delta_{ql}+\frac{\partial \overset{pq}{\phi}_k}{\partial Y_l}\right)\right]\delta_{jr} - \frac{\partial}{\partial Y_j}\left[L_{ijkl}(\lambda,\mathbf{Y})\overset{pq}{\phi}_k(\lambda,\mathbf{Y})\right]\delta_{lr}\Bigg\}\frac{\partial^2 \overset{0}{\bar{v}}_p}{\partial X_q\partial X_r}-\frac{\partial}{\partial Y_j}\left[L_{ijkl}(\lambda,\mathbf{Y})\frac{\partial \overset{1}{\bar{v}}_k}{\partial X_l}\right] \quad \text{(A.15)}$$

where the Euler–Lagrange equations corresponding to variational statement (A.13) were also used.

From $(A.13)_2$ and recalling (A.3) it can be seen that the right hand side of (A.15) is Y-periodic with zero average over the unit cell. Consequently from (A.2), and in analogy with the procedure followed in (A.10), $\overset{2}{\mathbf{v}}$ can be written in the following form

$$\overset{2}{v}_i(\lambda,\mathbf{X},\mathbf{Y})=\overset{pqr}{\psi}_i(\lambda,\mathbf{Y})\frac{\partial^2 \overset{0}{\bar{v}}_p}{\partial X_q\partial X_r}(\lambda,\mathbf{X})+\overset{pq}{\phi}_i(\lambda,\mathbf{Y})\frac{\partial \overset{1}{\bar{v}}_p}{\partial X_q}(\lambda,X)+\overset{2}{\bar{\mathrm{v}}}_i(\lambda,\mathbf{X}) \quad \text{(A.16)}_1$$

where

$$\frac{\partial}{\partial Y_j}\left[L_{ijkl}(\lambda,\mathbf{Y})\frac{\partial \overset{pqr}{\psi}_k}{\partial Y_l}\right]=\left[\mathscr{L}_{ijpq}(\lambda)-L_{ijkl}(\lambda,\mathbf{Y})\left(\delta_{pk}\delta_{ql}+\frac{\partial \overset{pq}{\phi}_k}{\partial Y_l}\right)\right]\delta_{ir}-\frac{\partial}{\partial Y_j}\left[L_{ijkl}(\lambda,\mathbf{Y})\overset{pq}{\phi}_k(\lambda,\mathbf{Y})\right]\delta_{lr};$$

$$\overset{pqr}{\psi} \text{ is } Y\text{-periodic}, \quad \int_D \overset{pqr}{\psi}\,\mathrm{d}\mathbf{Y}=0. \qquad (A.16)_2$$

It follows from (A.2) that $\overset{pqr}{\psi}$ are uniquely defined. It should be noted at this point that in deducing (A.16) from (A.15) we also made use of (A.11).

The $O(\varepsilon^1)$ term in the asymptotic expansion of (A.4) is

$$O(\varepsilon^1): \quad \int_{\mathbf{X}}\left[\int_D\left\{L_{ijkl}(\lambda,\mathbf{Y})\left(\frac{\partial \overset{1}{v}_k}{\partial X_l}+\frac{\partial \overset{2}{v}_k}{\partial Y_l}\right)\frac{\partial\delta v_i}{\partial X_j}+L_{ijkl}(\lambda,\mathbf{Y})\left(\frac{\partial \overset{2}{v}_k}{\partial X_l}+\frac{\partial \overset{3}{v}_k}{\partial Y_l}\right)\frac{\partial\delta v_i}{\partial Y_j}\right.\right.$$

$$\left.\left.-(\beta_0\overset{1}{v}_i+\beta_1\overset{0}{v}_i)\delta v_i\right\}\mathrm{d}\mathbf{Y}\right]\mathrm{d}\mathbf{X}=0. \qquad (A.17)$$

Adopting the same steps as in the analysis of the $O(\varepsilon^0)$ term (A.12), first $\delta \mathrm{v}_\mathrm{i}=\delta\bar{\mathrm{v}}_\mathrm{i}(\mathbf{X})$ is selected in (A.17). Substituting in (A.17) the expressions for $\overset{0}{\mathbf{v}}, \overset{1}{\mathbf{v}}$, and $\overset{2}{\mathbf{v}}$ in (A.8), (A.11), and $(A.16)_1$, and recalling the definition of $\mathscr{L}(\lambda)$ in $(A.13)_2$, the following variational statement for $\beta_1(\lambda)$ and $\overset{1}{\bar{\mathbf{v}}}(\lambda,\mathbf{X})$ is obtained

$$\int_{\mathbf{X}}\left\{\left[\mathscr{M}_{ijpqr}(\lambda)\frac{\partial^2\overset{0}{\bar{v}}_p}{\partial X_q\partial X_r}\frac{\partial\delta\bar{v}_i}{\partial X_j}-\beta_1(\lambda)\overset{0}{\bar{v}}_i\delta\bar{v}_i\right]+\left[\mathscr{L}_{ijpq}(\lambda)\frac{\partial\overset{1}{\bar{v}}_p}{\partial X_q}\frac{\partial\delta\bar{v}_i}{\partial X_j}-\beta_0(\lambda)\overset{1}{\bar{v}}_i\delta\bar{v}_i\right]\right\}\mathrm{d}\mathbf{X}=0, \qquad (A.18)_1$$

$$\mathscr{M}_{ijpqr}(\lambda)\equiv\frac{1}{\mathrm{vol}\,D}\int_D\left[L_{ijkl}(\lambda,\mathbf{Y})\left(\overset{pq}{\phi}_k(\lambda,\mathbf{Y})\delta_{lr}+\frac{\partial\overset{pqr}{\psi}_k}{\partial Y_l}\right)\right]\mathrm{d}\mathbf{Y}. \qquad (A.18)_2$$

In analogy to the analyses of (A.9) and (A.12), which provided the Y-dependence of $\overset{1}{\mathbf{v}}$ and $\overset{2}{\mathbf{v}}$, from (A.17) one can deduce the Y-dependence of $\overset{3}{\mathbf{v}}$. By appropriately rewriting the integrand of (A.17) and subsequently exploiting (A.3), one obtains

$$\int_{\mathbf{X}}\left[\frac{\partial}{\partial X_j}\left(\int_D\left\{L_{ijkl}(\lambda,\mathbf{Y})\left(\frac{\partial\overset{1}{v}_k}{\partial X_l}+\frac{\partial\overset{2}{v}_k}{\partial Y_l}\right)\delta v_i\right\}\mathrm{d}\mathbf{Y}\right)\mathrm{d}\mathbf{X}\right.$$

$$-\int_{\mathbf{X}}\left[\int_D\left\{\frac{\partial}{\partial X_j}\left[L_{ijkl}(\lambda,\mathbf{Y})\left(\frac{\partial\overset{1}{v}_k}{\partial X_l}+\frac{\partial\overset{2}{v}_k}{\partial Y_l}\right)\right]+\frac{\partial}{\partial Y_j}\left[L_{ijkl}(\lambda,\mathbf{Y})\left(\frac{\partial\overset{2}{v}_k}{\partial X_l}+\frac{\partial\overset{3}{v}_k}{\partial Y_l}\right)\right]\right.\right.$$

$$\left.\left.+(\beta_0\overset{1}{v}_i+\beta_1\overset{0}{v}_i)\right\}\delta v_i\mathrm{d}\mathbf{Y}\right]\mathrm{d}\mathbf{X}=0. \qquad (A.19)$$

In view of the arbitrariness of δv_i, and with the help of the Euler–Lagrange equations corresponding to $(A.13)_1$ and $(A.18)_1$, plus the expressions for $\overset{0}{\mathbf{v}}, \overset{1}{\mathbf{v}}, \overset{2}{\mathbf{v}}$, in (A.8), (A.11), (A.16), one obtains from (A.19) the following differential equations for $\overset{3}{\mathbf{v}}$

$$\frac{\partial}{\partial Y_j}\left[L_{ijkl}(\lambda,\mathbf{Y})\frac{\partial^3 v_k}{\partial Y_l}\right]=\left\{\left[\mathscr{M}_{ijpqr}(\lambda)-L_{ijkl}(\lambda,\mathbf{Y})\left(\overset{pq}{\phi}_k(\lambda,\mathbf{Y})\delta_{lr}+\frac{\partial \overset{pqr}{\psi}}{\partial Y_l}\right)\right]\delta_{js}\right.$$

$$\left.-\frac{\partial}{\partial Y_j}\left[L_{ijkl}(\lambda,\mathbf{Y})\overset{pqr}{\psi}_k(\lambda,\mathbf{Y})\right]\delta_{ls}\right\}\frac{\partial^3 \overset{0}{v}_p}{\partial X_q\partial X_r\partial X_s}$$

$$+\left\{\left[\mathscr{L}_{ijpq}(\lambda)-L_{ijkl}(\lambda,\mathbf{Y})\left(\delta_{pk}\delta_{ql}+\frac{\partial \overset{pq}{\phi}_k}{\partial Y_l}\right)\right]\delta_{jr}\right.$$

$$\left.-\frac{\partial}{\partial Y_j}\left[L_{ijkl}(\lambda,\mathbf{Y})\overset{pq}{\phi}_k(\lambda,\mathbf{Y})\right]\delta_{lr}\right\}\frac{\partial^2 \overset{1}{v}_p}{\partial X_q\partial X_r}$$

$$-\frac{\partial}{\partial Y_j}\left[L_{ijkl}(\lambda,\mathbf{Y})\frac{\partial \overset{2}{v}_k}{\partial X_l}\right]-\beta_0(\lambda)\overset{pq}{\phi}_i(\lambda,\mathbf{Y})\frac{\partial \overset{0}{v}_p}{\partial X_q}. \tag{A.20}$$

From (A.3), $(A.13)_2$ and $(A.18)_2$ it follows that the right hand side of (A.20) is Y-periodic with zero average over the unit cell. Hence from (A.2), and in analogy with the procedures followed in (A.10), (A.15), $\overset{3}{\mathbf{v}}$ can be written in the following form

$$\overset{3}{v}_i(\lambda,\mathbf{X},\mathbf{Y})=\overset{pqrs}{\theta}_i(\lambda,\mathbf{Y})\frac{\partial^3 \overset{0}{v}_p}{\partial X_q\partial X_r\partial X_s}(\lambda,\mathbf{X})-\beta_0(\lambda)\overset{pq}{\zeta}_i(\lambda,\mathbf{Y})\frac{\partial \overset{0}{v}_p}{\partial X_q}+\overset{pqr}{\psi}_i(\lambda,\mathbf{Y})\frac{\partial^2 \overset{1}{v}_p}{\partial X_q\partial X_r}(\lambda,\mathbf{X})$$

$$+\overset{pq}{\phi}_i(\lambda,\mathbf{Y})\frac{\partial \overset{2}{v}_p}{\partial X_q}(\lambda,\mathbf{X})+\overset{3}{\tilde{v}}_i(\lambda,\mathbf{X}), \tag{A.21}$$

where

$$\frac{\partial}{\partial Y_j}\left[L_{ijkl}(\lambda,\mathbf{Y})\frac{\partial \overset{pqrs}{\theta}_k}{\partial Y_l}\right]=\left[\mathscr{M}_{ijpqr}(\lambda)-L_{ijkl}(\lambda,\mathbf{Y})\left(\overset{pq}{\phi}_k(\lambda,\mathbf{Y})\delta_{lr}+\frac{\partial \overset{pqr}{\psi}_k}{\partial Y_l}\right)\right]\delta_{js}$$

$$-\frac{\partial}{\partial Y_j}\left[L_{ijkl}(\lambda,\mathbf{Y})\overset{pqr}{\psi}_k(\lambda,\mathbf{Y})\right]\delta_{ls};$$

$$\frac{\partial}{\partial Y_j}\left[L_{ijkl}(\lambda,\mathbf{Y})\frac{\partial \overset{pq}{\zeta}_k}{\partial Y_l}\right]=\overset{pq}{\phi}_i(\lambda,\mathbf{Y});\quad \overset{pqrs}{\boldsymbol{\theta}},\overset{pq}{\boldsymbol{\zeta}}\text{ are }Y\text{-periodic},\quad \int_D \overset{pqrs}{\boldsymbol{\theta}}\,d\mathbf{Y}=\mathbf{0},\quad \int_D \overset{pq}{\boldsymbol{\zeta}}d\mathbf{Y}=\mathbf{0}. \tag{A.21}_2$$

It follows from (A.2) that $\overset{pqrs}{\boldsymbol{\theta}}$ and $\overset{pq}{\boldsymbol{\zeta}}$ are uniquely defined. Note that in deducing (A.21) from (A.20), (A.11) and (A.16) were used.

The next (and last required for this presentation) order term $O(\varepsilon^2)$ in the asymptotic expansion of (A.4) is

$$O(\varepsilon^2):\quad \int_{\mathbf{x}}\left[\int_D\left\{L_{ijkl}(\lambda,\mathbf{Y})\left(\frac{\partial \overset{2}{v}_k}{\partial X_l}+\frac{\partial \overset{3}{v}_k}{\partial Y_l}\right)\frac{\partial\delta v_i}{\partial X_j}+L_{ijkl}(\lambda,\mathbf{Y})\left(\frac{\partial \overset{3}{v}_k}{\partial X_l}+\frac{\partial \overset{4}{v}_k}{\partial Y_l}\right)\frac{\partial\delta v_i}{\partial Y_j}\right.\right.$$

$$\left.\left.-(\beta_0(\lambda)\overset{2}{v}_i+\beta_1(\lambda)\overset{1}{v}_i+\beta_2(\lambda)\overset{0}{v}_i)\delta v_i\right\}d\mathbf{Y}\right]d\mathbf{X}=0. \tag{A.22}$$

By selecting once again $\delta v_i = \delta \bar{v}_i(\mathbf{X})$, substituting in (A.22) the expressions for $\overset{0}{\mathbf{v}}, \overset{1}{\mathbf{v}}, \overset{2}{\mathbf{v}}$, and $\overset{3}{\mathbf{v}}$ in (A.8), $(A.11)_1$, $(A.16)_1$ and $(A.21)_1$, and recalling the definitions for $\mathscr{L}(\lambda)$, $\mathscr{M}(\lambda)$ in $(A.13)_2$, $(A.18)_2$, the following variational statement for $\beta_2(\lambda)$ and $\overset{2}{\bar{\mathbf{v}}}(\lambda, \mathbf{X})$ is obtained

$$\int_{\mathbf{X}} \left\{ -\mathscr{N}_{ijspqr}(\lambda) \frac{\partial^3 \overset{0}{\bar{v}}_p}{\partial X_q \partial X_r \partial X_s} \frac{\partial \delta \bar{v}_i}{\partial X_j} - \beta_0(\lambda) \mathscr{S}_{ijpq}(\lambda) \frac{\partial \overset{0}{\bar{v}}_p}{\partial X_q} \frac{\partial \delta \bar{v}_i}{\partial X_j} - \beta_2(\lambda) \overset{0}{\bar{v}}_i \delta \bar{v}_i \right]$$

$$+ \left[\mathscr{M}_{ijpqr}(\lambda) \frac{\partial^2 \overset{1}{\bar{v}}_p}{\partial X_q \partial X_r} \frac{\partial \delta \bar{v}_i}{\partial X_j} - \beta_1(\lambda) \overset{1}{\bar{v}}_i \delta \bar{v}_i \right] + \left[\mathscr{L}_{ijpq}(\lambda) \frac{\partial \overset{2}{\bar{v}}_p}{\partial X_q} \frac{\partial \delta \bar{v}_i}{\partial X_j} - \beta_0(\lambda) \overset{2}{\bar{v}}_i \delta \bar{v}_i \right] \Bigg\} \mathrm{d}\mathbf{X} = 0, \quad (A.23)_1$$

$$\mathscr{N}_{ijspqr}(\lambda) \equiv -\frac{1}{\mathrm{vol}\, D} \int_D L_{ijkl}(\lambda, \mathbf{Y}) \left(\overset{pqr}{\psi}_k \delta_{ls} + \frac{\partial \overset{pqrs}{\theta}_k}{\partial Y_l} \right) \Bigg] \mathrm{d}\mathbf{Y}, \quad (A.23)_2$$

$$\mathscr{S}_{ijpq}(\lambda) \equiv \frac{1}{\mathrm{vol}\, D} \int_D L_{ijkl}(\lambda, \mathbf{Y}) \frac{\partial \overset{pq}{\zeta}_k}{\partial Y_l} \Bigg] \mathrm{d}\mathbf{Y}. \quad (A.23)_3$$

APPENDIX B: EXACT BIFURCATION CALCULATIONS FOR THE LAMINATED COMPOSITE

The analytical solution for the onset of bifurcation in a laminated composite under plane strain conditions has already been presented by Triantafyllidis and Maker (1985) for an incompressible solid with two different layers per unit cell and by Geymonant *et al.* (1993) for compressible solids with an arbitrary number of different material layers per unit cell. However, for reasons of completeness of the presentation, we give here a brief outline of the solution precedure which was used to find the microfailure surfaces and the corresponding critical modes in Figs 6–8.

The starting point for the analysis is the eigenvalue problem defining the critical load λ_c for the laminated medium. According to the general setting of the problem in Section 2.1, i.e. from $(2.4)_2$ and (2.5), the corresponding governing equations are

$$\frac{\mathrm{d}}{\mathrm{d}X_j} \left[L_{ijkl}(\lambda_c) \frac{\mathrm{d}v_k}{\mathrm{d}X_l} \right] = 0, \quad (B.1)_1$$

to which the following jump conditions have to be added at the layer interfaces, namely

$$\left[\left[L_{i2kl}(\lambda_c) \frac{\mathrm{d}v_k}{\mathrm{d}X_l} \right] \right] = 0, \quad [\![v_i]\!] = 0, \quad (B.1)_2$$

where $[\![f]\!]$ denotes the difference in the values of f when evaluated at both sides of an interface $X_2 = c$.

Since the incremental moduli $L_{ijkl}(\lambda)$ of the composite are (piecewise constant) functions of X_2, we can show [see Geymonant *et al.* (1993)] that the eigenmode v_k takes the form

$$v_k(X_1, X_2) = \exp(\mathrm{i}\omega_1 X_1) \hat{v}_k(X_2), \quad \hat{v}_k(X_2) = \exp(\mathrm{i}\omega_2 X_2) p(X_2), \quad (B.2)$$

where $\mathrm{i} = \sqrt{-1}$ and $p(X_2)$ is a (piecewise constant) periodic function of X_2 with period the unit cell thickness H. Substituting $(B.2)_1$ into $(B.1)_1$ yields a system of ordinary differential equations in X_2 with piecewise constant coefficients. The solution of these ordinary differential equations gives the following results for $\hat{v}_k$

$$\hat{v}_k(X_2) = \sum_{j=1}^{4} C_k^j \exp(\mathrm{i}\omega_1 z_j X_2), \quad (B.3)_1$$

where C_k^l are constants in each layer and z_j are the four complex roots of the following biquadratic polynomial (the z_j are also constant in each layer)

$$(L_{1212}L_{2222})z_j^4+[L_{1111}L_{2222}+L_{1212}L_{2121}-(L_{1122}+L_{1221})^2]z_j^2+(L_{1111}L_{2121})=0, \quad (j=1,4). \tag{B.3}_2$$

The complexity of the roots z_j is assured by the strong ellipticity property holding for each layer [see discussion of (4.10)].

By introducing the above found expressions for $\hat{v}_k$ into the interface conditions $(B.1)_2$ and exploiting $(B.2)_2$, one concludes (after some considerable algebraic manipulations) that a non-trivial solution ($C_j^k \neq 0$) can be found if the load parameter λ satisfies

$$\mathrm{Det}[\mathbf{F}(\lambda,\omega_1 H)-\exp(i\omega_2 H)\mathbf{I}]=0. \tag{B.4}_1$$

where $\mathbf{I}$ is the 4×4 identity matrix and where the 4×4 matrix $\mathbf{F}(\lambda,\omega_1 H)$ is given by

$$\mathbf{F}\equiv K_f\mathbf{K}_m, \quad \mathbf{K}_l\equiv \mathbf{V}_l\exp[i\omega_1 H_l\mathbf{Z}_l]\mathbf{V}_l^{-1}, \quad \mathbf{Z}_l\equiv \mathrm{diag}[z_j]_l, \quad (l=\mathrm{m\ or\ f}), \tag{B.4}_2$$

and where the components of the 4×4 matrix $\mathbf{V}_l$ are defined in each layer by

$$\begin{aligned}
V_{1j}&=1,\\
V_{2j}&=(L_{1111}+z_j^2L_{1212})/[z_j(L_{1122}+L_{1221})],\\
V_{3j}&=z_jL_{1212}-L_{1221}[(L_{1111}+z_j^2L_{1212})]/[z_j(L_{1122}+L_{1221})],\\
V_{4j}&=L_{1122}-L_{2222}[(L_{1111}+z_j^2L_{1212})]/(L_{1122}+L_{1221}).
\end{aligned} \tag{B.4}_3$$

The critical load parameter λ_c corresponding to the first bifurcation of the laminated solid is the minimum/maximum (for $\lambda>1/\lambda<1$) root of the characteristic equation $(B.4)_1$, where the corresponding extremum is taken over all possible values of the wavenumbers, i.e. $0<\omega_1 H<+\infty$, $0<\omega_2 H<2\pi$.

After some considerable algebraic manipulations of (B.4), it can be shown that the following three possibilities exist, according to the value of $(\omega_2 H)_c$ at the critical load λ_c

$$\begin{aligned}
&2I_1^F(\lambda,\omega_1 H)-I_2^F(\lambda,\omega_1 H)-2=0, \quad (\omega_2 H)_c=0,\\
&2I_1^F(\lambda,\omega_1 H)+I_2^F(\lambda,\omega_1 H)+2=0, \quad (\omega_2 H)_c=\pi,\\
&(1/4)[I_1^F(\lambda,\omega_1 H)]^2-I_2^F(\lambda,\omega_1 H)+2=0, \quad (\omega_2 H)_c=\pm\cos^{-1}(I_1^F/4),
\end{aligned} \tag{B.5}_1$$

where I_1^F and I_2^F are the first two invariants of the matrix $\mathbf{F}$ defined in $(B.4)_2$, namely

$$I_1^F\equiv \mathrm{tr}\,\mathbf{F}, \quad I_2^F\equiv(1/2)[(\mathrm{tr}\,\mathbf{F})^2-\mathrm{tr}\,\mathbf{F}^2]. \tag{B.5}_2$$

The wanted critical load parameter λ_c is then found as the extremum (minimum/maximum) root among the corresponding extremal roots of the three equations in $(B.5)_1$, when the extremum is taken over all the positive real numbers for $\omega_1 H$.